A Live Attenuated Vaccine Candidate against Emerging Highly Pathogenic Cattle-Origin 2.3.4.4b H5N1 Viruses

Ahmed Mostafa[1,2,*], Chengjin Ye[1], Ramya S. Barre[1], Vinay Shivanna[3], Reagan Meredith[4], Roy N. Platt[1], Ruby A. Escobedo[1], Mahmoud Bayoumi[1,5], Esteban M. Castro[1], Nathaniel Jackson[1], Anastasija Cupic[6,7], Aitor Nogales[8], Timothy J. C. Anderson[1], Adolfo García-Sastre[7,9,10,11,12,13], Luis Martinez-Sobrido[1,*]

[1] Host-pathogen interactions (HPI) and Disease Intervention and Prevention (DIP) programs, Texas Biomedical Research Institute, San Antonio, TX 78227, USA.

[2] Center of Scientific Excellence for Influenza Viruses, National Research Centre, Giza 12622, Egypt.

[3] Southwest National Primate Research Center at the Texas Biomedical Research Institute, San Antonio, TX 78227, USA.

[4] Population Health and Host Pathogen Interactions Programs, Texas Biomedical Research Institute, San Antonio, TX, USA

[5] Virology Department, Faculty of Veterinary Medicine, Cairo University, Giza, Egypt.

[6] Graduate School of Biomedical Sciences, Icahn School of Medicine at Mount Sinai, New York, NY, USA.

[7] Department of Microbiology, Icahn School of Medicine at Mount Sinai, New York, NY, USA.

[8] Center for Animal Health Research, CISA-INIA-CSIC, Madrid, Spain.

[9] Global Health and Emerging Pathogens Institute, Icahn School of Medicine at Mount Sinai, New York, NY, USA.

[10] Department of Medicine, Division of Infectious Diseases, Icahn School of Medicine at Mount Sinai, New York, NY, USA.

[11] The Tisch Cancer Institute, Icahn School of Medicine at Mount Sinai, New York, NY, USA.

[12] Department of Pathology, Molecular and Cell-Based Medicine, Icahn School of Medicine at Mount Sinai, New York, NY, USA.

[13] The Icahn Genomics Institute, Icahn School of Medicine at Mount Sinai, New York, NY, USA.

* Correspondence should be addressed to:

Luis Martinez-Sobrido (lmartinez@txbiomed.org; https://orcid.org/0000-0001-7084-0804)

Ahmed Mostafa, PhD (aelsayed@txbiomed.org; https://orcid.org/0000-0002-2878-5714)

Abstract

Influenza viruses present a significant public health risk, causing substantial illness and death in humans each year. Seasonal flu vaccines must be updated regularly, and their effectiveness often decreases due to mismatches with circulating strains. Furthermore, inactivated vaccines do not provide protection against shifted influenza viruses that have the potential to cause a pandemic. The highly pathogenic avian influenza H5N1 clade 2.3.4.4b is prevalent among wild birds worldwide and is causing a multi-state outbreak affecting poultry and dairy cows in the United States (US) since March 2024. In this study, we have generated a NS1 deficient mutant of a low pathogenic version of the cattle-origin human influenza A/Texas/37/2024 H5N1, namely LPhTXdNS1, and validated its safety, immunogenicity, and protection efficacy in a prime vaccination regimen against wild-type (WT) A/Texas/37/2024 H5N1. The attenuation of LPhTXdNS1 *in vitro* was confirmed by its reduced replication in cultured cells and inability to control IFNβ promoter activation. In C57BL/6J mice, LPhTXdNS1 has reduced viral replication and pathogenicity compared to WT A/Texas/37/2024 H5N1. Notably, LPhTXdNS1 vaccinated mice exhibited high immunogenicity that reach its peak at weeks 3 and 4 post-immunization, leading to robust protection against subsequent lethal challenge with WT A/Texas/37/2024 H5N1. Altogether, we demonstrate that a single dose vaccination with LPhTXdNS1 is safe and able to induce protective immune responses against H5N1. Both safety profile and protection immunity suggest that LPhTXdNS1 holds promise as a potential solution to address the urgent need for an effective vaccine in the event of a pandemic for the treatment of infected animals and humans.

Keywords: H5N1 virus; vaccine; live attenuated vaccine; NS1; deltaNS1; immunogenicity; Highly pathogenic avian influenza virus.

Introduction

H5N1 avian influenza virus clade 2.3.4.4b emerged in 2020 and became dominant in Asia, Europe, and Africa by 2021. It spread to North America by the end of 2021, causing poultry outbreaks, and reached Central and South America in 2022, affecting farmed animals, mammals, and wildlife. In March 2024, a new genotype (B3.13) of H5N1 clade 2.3.4.4b emerged in the United States (US) to infect birds and dairy cattle, marking the first outbreak of H5N1 in ruminants (1). Shortly after, a human case was reported in a dairy farm worker in Texas following exposure to infected cattle, representing the first cattle-to-human transmission of H5N1 (1). Successively, H5N1 clade 2.3.4.4b genotype B3.13 resulted in massive outbreaks in cattle farms in the majority of the US, with remarkable increase in cattle-to-human transmission (1, 2). Amidst a yearlong H5N1 clade 2.3.4.4b genotype B3.13 outbreak in cattle farms, a second H5N1 clade 2.3.4.4b genotype D1.1 was also identified in early 2025 in cattle after transmission from birds (3).

Seasonal influenza vaccines reduce the burden of influenza disease, but their overall effectiveness varies each year (approximately 30-67%) (4-7), depending on how well the vaccine strain matches the circulating influenza viruses. Moreover, waning effectiveness has also been observed just a few months following vaccination, resulting in remarkable reductions in protection likely due to bias following the emergence of antigenic drift variants of influenza viruses that are not well-matched to the vaccine strains (7). In addition, the inactivated influenza vaccines induce a suboptimal immune response, especially when vaccine strains do not match circulating viruses, and fail to stimulate mucosal immunity, which could offer better protection against respiratory infections (8). Recent studies have shown that seasonal vaccination can boost antibody titers to protective levels in a moderate percentage of individuals against avian influenza viruses, likely due to cross-reactive immune responses (9, 10). These findings highlight the importance of vaccination and suggest that seasonal influenza vaccines could serve as an initial defense against a potential pandemic caused by avian influenza viruses, followed using more specific pandemic vaccines. Also, they highlight the significance of replacing the current inactivated vaccines with more effective live-attenuated influenza vaccines (LAIVs). LAIVs, which are recommended for individuals between the ages of 2 and 49, can trigger a range of immune responses by simulating a natural infection through

intranasal administration, resulting in more robust and long-lasting immunity and protective effectiveness.

The current attenuated (*att*), temperature-sensitive (*ts*), cold-adapted (*ca*) 6+2 influenza virus reassortant seasonal LAIV based on the genetic background of influenza A/Ann Arbor/6/60 H2N2 (AA), has shown varying levels of effectiveness (11). The variable effectiveness of LAIVs is sometimes attributed to different factors, including improper selection of the vaccine strain, the attenuation method (12), or limitations in accurately assessing effectiveness due to limited use (11). The reduced effectiveness of seasonal LAIV in recent years may be also due to mismatching between the internal genes of the current LAIV strain, which are derived from viruses isolated between 1957 and 1960, and the currently circulating influenza viruses (13). Nonetheless, reports indicate that LAIVs can be up to 85% effective in children with a neutralizing antibody response durability for up to six months after vaccination (14-16). However, in adults, ca LAIV is poorly immunogenic, due to hyperattenuation of LAIV in the presence of immunity acquired by previous exposures to circulating influenza viruses (12, 17, 18).

The non-structural protein 1 (NS1) of influenza A virus (IAV) is crucial for interacting with many host proteins, suppressing the host's antiviral response, and promoting viral replication and pathogenicity (19-21). IAV lacking NS1 are significantly weakened, making them viable for use as LAIVs (22). NS1-deficient (dNS1) LAIVs can mimic natural infection, induce robust immune responses, and protect against wild-type (WT) virus challenge, making them a promising option for emerging zoonotic avian influenza viruses (8). Recombinant avian, equine, canine, and swine IAV with partial truncations or deficiency in NS1 have been generated and proposed as potential LAIVs in diverse animal models including mice, guinea pigs, ferrets, chickens, horses, and dogs (13, 23).

Here, we investigated the impact of NS1 deletion on the replication, pathogenicity, virus-induced cellular and humoral responses, and protection efficacy of a low pathogenic cattle-origin human influenza A/Texas/37/34 H5N1 (LPhTXdNS1). Our results demonstrate that mice vaccinated with a single internasal dose of LPhTXdNS1 remain free of clinical signs of infection, exhibit strong immunogenicity, and protects against a subsequent lethal challenge with WT A/Texas/37/2024 H5N1, supporting its potential as

an effective LAIV for combating the recent cattle-origin H5N1 highly pathogenic avian influenza virus (HPAIV) in the event of a pandemic.

Materials and Methods

Biosafety

All *in vitro* and *in vivo* studies involving highly pathogenic and low pathogenic avian influenza virus (HPAIV and LPAIV, respectively) H5N1 were conducted at biosafety level (BSL) 3 and animal BSL3 (ABSL3) laboratories at Texas Biomedical Research Institute (Texas Biomed). These experiments were approved by both the Texas Biomed Institutional Biosafety (IBC) and the Animal Care and Use (IACUC) committees.

Cells

Madin-Darby canine kidney (MDCK), human embryonic kidney (293T), African green monkey kidney (Vero), and MDCK cells expressing GFP and firefly luciferase (FFluc) under the control of the interferon (IFN) β promoter (MDCK pIFNβ-GFP/IFNβ-FFluc) (24) were cultured in Dulbecco's modified Eagle medium (DMEM) (Invitrogen, USA) complemented with 10% fetal bovine serum (FBS) and 1% PSG (penicillin, 100 U/mL; streptomycin, 100 µg/mL; L-glutamine, 2 mM). Cultured cells were kept at 37°C in a humidified 5% CO_2 incubator.

Plasmids and viruses

The recombinant low pathogenic human influenza virus A/Texas/37/2024 H5N1 (LPhTX) was generated as previously described (25) and propagated in MDCK cells using infection media (DMEM containing 1% P/S/G and 0.2% BSA) in the presence of 1 µg/mL of L-1-tosylamido-2-phenylethyl chloromethyl ketone (TPCK)-treated trypsin (Sigma–Aldrich, USA).

The pHW-hTX_NS plasmid (25), which expresses the NS1 and nuclear export protein (NEP) of A/Texas/37/2024 H5N1, was used as a template to remove the NS1-coding sequence. Briefly, 2 µl (5 ng/µl) of pHW-hTX_NS were combined with 5 µl of 10X Pfu reaction buffer, 1 µl of 10 mM dNTP mixture (0.2 mM of each), 1.5 µl of 50 mM MgCl2 (1.5 mM), 2 µl of forward primer (F: GTTAAGCTTTCAGGACATACTGATGAGGATGTCAAAAATGCAATTGGGGTCCTCAT)

154 (40 pmoles), 2 µl of reverse primer (R:
155 CTGAAAGCTTAACACAGTGTTGGAATCCATTATGTTTTTGTCACCCT) (40 pmoles),
156 and 1 µl of PfuTurbo DNA Polymerase (2.5 U/µl) (Invitrogen, USA). The total volume was
157 adjusted to 50 µl using nuclease-free water (Ambion, USA). The reaction was preceded
158 by a pre-denaturation at 95°C for 2 min, followed by 35 PCR cycles (95°C for 30 sec for
159 denaturation, 56°C for 30 sec for annealing, and 72°C for 3 min for extension), and a final
160 extension step at 72°C for 10 min. The PCR product was purified using the Wizard® SV
161 Gel and PCR Clean-Up System (Promega, USA). The resulting PCR product was then
162 digested with HindIII (NEB, USA) to create the pHW-hTX-dNS1 plasmid.
163 To generate LPhTXdNS1, the seven ambisense pHW2000 plasmids containing the
164 PB2, PB1, PA, monobasic HA, NP, NA, and M segments of LPhTX, and the pHW-hTX-
165 dNS1 plasmid (1 µg each) were co-transfected into a 293T/MDCK cell co-cultures (3:1
166 ratio) using Lipofectamine™ 3000 Transfection Reagent (ThermoFisher Scientific, USA),
167 according to the manufacturer's protocol. After 24 h, the transfection medium was
168 replaced with 1 mL of Opti-MEM media containing 1% PSG and 0.2% bovine serum
169 albumin (BSA) and the culture was incubated in a 5% CO_2 incubator. Twelve hours later,
170 an additional 1 mL of Opti-MEM media containing 1% PSG, 0.2% BSA, and 2 µg/mL of
171 TPCK-treated trypsin was added to each well. After 48-72 h, cell culture supernatants
172 were harvested and centrifuged at 2,500 rpm for 5 min at 4°C. A portion of the collected
173 supernatant was used to infect MDCK monolayers in T-75 cell culture flasks in infection
174 media (DMEM with 1% PSG, 0.2% BSA, and 2 µg/mL of TPCK-treated trypsin). The
175 rescued LPhTXdNS1 was then aliquoted and stored at −80°C.
176 Viral stock was confirmed by whole genome sequencing using the MinION platform
177 (Oxford Nanopore Technologies) in comparison to the generated LPhTX strain. Briefly,
178 viral RNA was extracted using the QiAamp Viral RNA Mini Kit (Qiagen, USA), and sample
179 libraries were prepared with the Native Barcoding Kit 24 V14 (SQK-NBD114.24, Oxford
180 Nanopore Technologies). Sequencing was performed on R10.4.1 Flow Cells (FLO-
181 MIN114, Oxford Nanopore Technologies) according to the manufacturer's instructions.
182 Following nanopore sequencing, the initial read quality statistics were evaluated using
183 n50 v1.7.0, followed by quality filtering with nanoq v0.10.0 (26). Reads were trimmed once
184 average PHRED quality scores dropped below Q<10. In addition, we removed the first

185 and last 15 base pairs of each read. After trimming, reads shorter than 500 base pairs
186 were completely removed. Quality-trimmed reads were polished using the self-correcting
187 algorithm LoRMA v0.4.2 (27) by comparing batches of 100 overlapping reads. Polished
188 reads were aligned to the H5N1 LPhTX reference genome using minimap2 v2.28-r1209
189 (28) with the -x map-ont parameter to optimize mapping of error-prone, long Nanopore
190 reads. Alignment statistics were calculated using SAMtools flagstat v1.21 (29), and
191 genome-wide coverage was estimated using MosDepth v0.3.10 (30). We used LoFreq
192 v2.1.5 (31) to evaluate indel quality and identify sequence variants. For variant calling,
193 we capped the maximum allowable read depth at 10,000x (--max-depth) and disabled
194 LoFreq's default filters. Instead, we applied custom filtering criteria, retaining only variants
195 supported by at least 25% of reads and located in regions with a minimum read depth of
196 100x.We also removed indels caused by homopolymer runs of three or more bases. For
197 reproducibility, all analyses were completed on worker nodes containing 192 cores and
198 1Tb of memory at the Texas Biomedical Research Institutes high-performance computing
199 center. All code necessary to complete the genetic analysis is available at GitHub
200 (https://github.com/nealplatt/h5n1_highpathcow_2025-03-17). Sequence data is
201 archived under BioProject accession code "PRJNA1242379".
202 A recombinant A/Texas/37/2024 H5N1 containing a non-structural (NS) segment where
203 the C-terminus of NS1 was fused to Nanoluciferase (NLuc) was engineered as previously
204 described (32). The recombinant NS segment was synthesized *de novo* (Bio Basic, USA)
205 with the appropriate restriction sites for subcloning into the ambisense plasmid pHW200
206 to generate the pHW-H5N1-NS_AgeI/NheI plasmid. The recombinant NS segment
207 contained the NS1 open reading frame (ORF) without stop codons or splice acceptor
208 sites, followed by AgeI and NheI restriction sites, the porcine teschovirus-1 (PTV-1) 2A
209 autoproteolytic cleavage site (ATNFSLLKQAGDVEENPGP) and the entire ORF of the
210 nuclear export protein, NEP (33). The Nluc ORF was cloned using the AgeI and NheI
211 sites, into pHW-H5N1-NS_AgeI/NheI to generate the pHW-H5N1-NS_Nluc for virus
212 rescue. Plasmid constructs were confirmed by DNA sequencing (Plasmidsaurus, USA).
213 Recombinant A/Texas/37/2024(H5N1) virus expressing NS1_Nluc (HPhTX-Nluc) was
214 rescued as previously described (25, 34-37). HPhTX-Nluc was then plaque purified and
215 amplified on MDCK cells to generate the viral stock.

216 **Plaque Assay and Immunostaining**

217 MDCK and Vero cells were seeded at a density of 10^6 cells per well in 6-well plates
218 and incubated overnight at 37°C in a humidified 5% CO_2 incubator. The following day, the
219 confluent MDCK monolayers were infected with 10-fold serial dilutions of the virus for 1 h
220 at 37°C. After viral adsorption, the cell monolayers were overlaid with post-infection media
221 containing agar and incubated at 37°C in a humidified 5% CO_2 incubator. At 24
222 (immunostaining) and 72 (plaque assay) hours post-infection (hpi), cells were fixed for 24
223 h with 10% neutral buffered formalin. For staining and visualization of viral plaques with
224 crystal violet, 1 mL of 0.1% crystal violet solution was applied to each well for 5 min at
225 room temperature (RT), followed by rinsing with tap water. For immunostaining, cells were
226 permeabilized with 0.5% Triton X-100 in PBS for 15 min at RT and stained with the mouse
227 monoclonal antibody (MAb) HT103 against influenza viral nucleoprotein (NP) (38) and
228 the Vectastain ABC kit (Vector Laboratories, USA), following the manufacturer's protocol.
229 After immunostaining, the plates were scanned and photographed using the ChemiDoc
230 MP Imaging System.

231 **Western blotting**

232 Vero cell monolayers (6-well plate format, 10^6 cells/well, triplicates) were infected with
233 LPhTX and LPhTXdNS1 at multiplicity of infection (MOI) of 2. At 12 hpi, cells were washed
234 with ice-cold PBS and treated with ice-cold NP40 lysis buffer (Thermo; completed with
235 protease inhibitors cocktail). Cells were lysed on ice for 30 min, scrapped off and
236 transferred to 1.5 mL Eppendorf tubes. Cells were centrifuged at 15,000 rpm for 15 min
237 at 4°C. The cell lysate supernatants were then mixed with 2x working lithium dodecyl
238 sulfate (LDS) sample buffer, supplemented with 20% β-mercaptoethanol and incubated
239 at 98°C for 5 min before loading into SDS-PAGE gels. Following sample running, gels
240 were transferred into nitrocellulose membranes. Subsequently, membranes were
241 incubated in 5% non-fat dry milk powder in PBS with 0.05% Tween 20 blocking buffer
242 (PBST) (Sigma, USA). Blocked membranes were probed overnight at 4°C with primary
243 antibodies against PB1 (Clone F5-46, BEI Resources), PA (Clone 1F6, BEI Resources),
244 NP (HT103) (38), NS1 (pAb, 1-73SW) (13), and β-actin (clone AC-15; A1978; Sigma,
245 USA) as a house keeping protein. After overnight incubation, membranes were washed
246 3x for 5 min each with 5 mL of PBST. After washing, membranes were incubated with

247 HRP-conjugated secondary antibodies for 2 h at RT. After 3x washes for 5 min with 5 mL
248 of PBST, chemiluminescence-generated protein bands were visualized using a
249 SuperSignal ECL substrate kit (ThermoFisher, USA) following manufacturer's
250 recommendations.

251 **Viral replication kinetics**

252 Vero cell monolayers cultured in 6-well plates (10^6 cells per well, triplicates) were
253 infected with the specified viruses at a MOI of 0.001 and plates were kept at 37°C or 33°C
254 in a humidified 5% CO_2 incubator for 1 h to allow viral adsorption. After viral adsorption,
255 the inoculum was removed and infected cell monolayers were washed 3x with PBS to
256 eliminate any unadsorbed viral particles. Cell monolayers were then supplemented with
257 3 mL of infection medium containing 2 ug/mL of TPCK-treated trypsin and incubated at
258 37°C in a humidified 5% CO_2 incubator. Aliquots of 200 µL were taken from the cell culture
259 supernatants at 12, 24, 48, and 72 hpi and replaced with an equal volume of fresh
260 infection medium. Viral titers in the collected samples were determined using plaque
261 assays and immunostaining, as previously described (25, 39).

262 **Mice experiments**

263 Female C57BL/6J mice (n=13/group) obtained from The Jackson Laboratory (JAX,
264 USA) were anesthetized intraperitoneally (i.p.) by a cocktail of Ketamine (100 mg/mL) and
265 Xylazine (20 mg/mL). Anesthetized mice were infected intranasally (i.n.) with the
266 indicated viral doses in a total volume of 50 µl PBS. On 2-, 4-, and 6-days post-infection
267 (DPI), 4 mice in each group were humanely euthanized to collect lung, nasal turbinate,
268 and brain tissues. Half of the lung and brain organs were fixed in 10% neutral buffered
269 formalin solution for histopathology and immunohistochemistry (IHC) analyses, and the
270 other halves were homogenized in 1 mL of PBS using a Precellys tissue homogenizer
271 (Bertin Instruments, USA) for viral titration. Tissue homogenates were centrifuged at
272 10,000 *xg* for 5 min and the supernatants were used to determine viral load by plaque
273 assay and investigate the presence of secreted cytokines/chemokines. The remaining 5
274 mice/group were monitored for 14 days for body weight changes (morbidity), and survival
275 rates (mortality). Mice that experienced a weight loss exceeding 25% of their original
276 weight were humanely euthanized.

277 **Hemagglutination inhibition (HAI) assay**

278 Sera were collected weekly from both mock-vaccinated and vaccinated mice (n =
279 5/group). The sera were treated with receptor-destroying enzyme (II) (RDE-II, Denka
280 Seiken, USA) for 20 h at 37°C. The RDE-II enzyme was inactivated by heating at 56°C
281 for 30 min. After treatment, 12.5 µl of the sera was added in triplicate to 96-well plates
282 and mixed with 12.5 µl of diluted LPhTX, containing 4 hemagglutinating (HA) units. The
283 plates were incubated for 30 min at RT. Then, 25 µl of 1% turkey red blood cells (RBCs)
284 was added to each well, and after 45 min HAI was determined as the highest dilution of
285 antiserum that completely inhibited hemagglutination (40).

286 **Histopathology and immunohistochemistry (IHC)**

287 Mice lung and brain tissues were collected at necropsy, fixed in 10% neutral buffered
288 formalin and processed in a Tissue Tek VIP tissue processor, where they were dehydrated
289 through a series of graded alcohols, cleared with a 50:50 absolute alcohol/xylene mixture
290 and two changes of xylene, and then infiltrated with paraffin wax using ParaPro™ XLT
291 infiltration and embedding media (StatLab, USA). The paraffin blocks were sectioned at
292 4 microns thick using a Microm HM325 rotary microtome and mounted on microscope
293 slides using a flotation water bath set between 46° and 48°C. The slides were then placed
294 in a Varistain Gemini automated slide stainer for H&E staining, followed by drying in
295 heating stations before the staining program began. The deparaffinization of tissue
296 sections was done with three changes of xylene, two changes of absolute alcohol, and
297 two changes of 95% alcohol, followed by rinsing in distilled water. Hematoxylin staining
298 was conducted with Reserve Bluing Reagent (StatLab, USA), with excess stain removed
299 using High-Def solution (StatLab, USA). The tissue sections were then stained with Eosin
300 (StatLab, USA), dehydrated in three changes of alcohol, a 50:50 absolute alcohol/xylene
301 mixture, and cleared in three changes of xylene before mounting them in coverslips. After
302 staining, the tissue sections were examined by a board-certified veterinary pathologist in
303 a blinded fashion. For IHC, tissue sections were cut at 4 microns, mounted onto positively
304 charged slides, and allowed to air dry overnight. The slides were then processed using
305 the Discovery Ultra IHC/ISH automatic stainer to detect avian influenza virus.
306 Deparaffinization was performed using Discovery Wash (Roche, USA). Cell conditioning
307 was done with Discovery CC1 (Roche, USA) at 95°C for 64 min. Endogenous peroxidase

308 was blocked with Discovery Inhibitor (Roche, USA) for 8 min. Slides were then incubated
309 with a rabbit polyclonal antibody against IAV NP (Invitrogen, USA) at a 1:1,500 dilution
310 for 1 h at RT, followed by detection with an anti-rabbit HQ (Roche, USA) for 8 min, and
311 anti-HQ HRP (Roche, USA) for 8 min at 36°C. Influenza NP was visualized using
312 ChromoMAP DAB (Roche, USA). The slides were counterstained with Hematoxylin
313 (Roche, USA) and blued using Bluing Reagent (Roche, USA). All HE stained and IHC
314 stained slides were scanned using Zeiss axio scan. Z1 whole slide scanner at ×20
315 magnification. The digital slides were analyzed using an AI optimized tissue classifier in
316 HALO v4.0 software (Indica Labs, USA) for absolute quantification of the percentage of
317 lung affected and percentage of lung staining for viral antigen.

318 **Statistical analyses**

319 All graphs, calculations, and statistical analyses were performed using GraphPad
320 Prism software version 9.5.1 (GraphPad Software, LLC, USA). No assumptions of equal
321 variance or sphericity were made for group comparisons. Normality of residuals was
322 checked for all group comparisons and log10 transformations were applied when the
323 assumption of normality was not met. Growth kinetics were analyzed using a two-way
324 repeated measure ANOVA with Geisser-Greenhouse correction. Post-hoc comparisons
325 were performed using the Šídák method. Differences in FFluc expression were evaluated
326 using Welch's one-way ANOVA, followed by multiple comparisons using Dunnett T3
327 method. Viral replication and titer data were analyzed using two-way repeated measure
328 ANOVA with Geisser-Greenhouse correction. Post-hoc testing was conducted with
329 Dunnett's multiple comparisons test. Differences in survival curves were analyzed using
330 a Log-rank test.

331

332 **Results**

333 **Generation and characterization of LPhTXdNS1**

334 IAV NS1 has been previously described to inhibit host gene expression, including type
335 I interferon (IFN-I) responses and, therefore, contribute to viral virulence (20, 21). To
336 establish an attenuated recombinant low pathogenic influenza A/Texas/37/2024 H5N1
337 with the potential to be implemented as a LAIV, we conducted virus attenuation by
338 removing two key virulence viral factors, the NS1 protein and the multibasic cleavage site

339 (PLREKRRKR/GLF) in the viral HA protein (**Fig. 1a**). Using our previously described
340 reverse genetics for influenza A/Texas/37/2024 H5N1, we generated LPhTXdNS1, a virus
341 lacking the NS1 protein and expressing a monobasic cleavage site (PQIETR/GLF) in the
342 HA protein. We also generated a control A/Texas/37/2024 H5N1 virus, which has a
343 monobasic cleavage site in its HA protein, but with an intact NS1 protein (LPhTX) (**Fig.**
344 **1a**).

345 After rescuing LPhTXdNS1, the lack of NS1 expression was confirmed by Western
346 blot (**Fig. 1b**) and next generation sequencing (**Fig. 1c**). In LPhTXdNS1-infected Vero cell
347 lysates, the polymerase subunits PB1 and PA, and the viral NP, were detected at similar
348 levels using specific antibodies in both LPhTXdNS1- and LPhTX-infected cells (**Fig. 1b**).
349 However, NS1 expression was undetectable with an anti-NS1 antibody in Vero cell lysates
350 infected with LPhTXdNS1 (**Fig. 1b**), contrary to LPhTX-infected Vero cells where NS1
351 expression was readily detectable.

352 On the same hand, the long-read sequencing data generated from Nanopore runs for
353 LPhTX and LPhTXdNS1 were summarized in **Table 1**. In total, we analyzed 131.1
354 megabases (Mb). Read depth ranged from 427x-889x (**Table 1; Fig. 1c**). Reduced
355 coverage in the LPhTXdNS1 gene was due, in part, to the dNS1 deletion. We identified
356 21 variants in the HA and NS segments after applying filtering criteria that removed
357 variants with allele frequencies below 25% (**Table 2; Fig. 1d**). Of these, 14 were indels
358 associated with homopolymer regions greater than 3 nt in length which are known to pose
359 challenges for accurate sequencing using Nanopore technology (41). The frequencies of
360 the remaining 7 variants were below 50% in each sample (**Table 2**). Among these seven
361 non-silent variants, six (HA: G539A, C1068T; NS: C201G, C440G, C444T, and G445A)
362 were associated with LPhTX, while only one variant (G539A) was linked to LPhTXdNS1.

363 The plaque sizes of LPhTXdNS1 in Vero cells at 33°C and 37°C was slightly smaller
364 than LPhTX, containing a functional NS1 protein (**Fig. 1e**). To confirm that LPhTXdNS1
365 is limited in its ability to replicate in immunodeficient but not in immunocompetent cells,
366 we conducted plaque assays of LPhTXdNS1 in MDCK and Vero cells, respectively, at
367 33°C and 37°C for 48 hpi. No viral plaques were detected in MDCK cells, whereas
368 LPhTXdNS1 was able to form plaques in Vero cells (**Fig. 1f**). As expected, the
369 LPhTXdNS1 replicates in IFN-I deficient Vero cells, reaching viral peaks at ~48 hpi to

370 average titers of $1.7x10^5$ and $1.467x10^7$ PFU/ml at 33°C and 37°C, respectively (**Fig. 1g**)
371 that is ~30 and ~12 times lower than LPhTX at same corresponding temperatures,
372 respectively. Altogether, these results demonstrate that NS1 deletion in LPhTXdNS1
373 renders the virus attenuated *in vitro* when compared to the NS1-expressing LPhTX virus.

374 **LPhTXdNS1 lacks the ability to inhibit IFNβ promoter activation.**

375 We further confirmed the lack of NS1 expression by LPhTXdNS1 by infecting MDCK
376 cells constitutively expressing GFP-CAT and FFluc under the control of an IFNβ promoter
377 (24), designated hereafter as MDCK IFNβ GFP-CAT/FFluc (**Fig. 2a**). As expected, LPhTX
378 was able to efficiently control IFNβ promoter activation as determined by the lack of GFP
379 and reduced FFluc expression (**Figs. 2b-c**). However, cells infected with LPhTXdNS1
380 showed high levels of GFP and FFluc expression, compared to LPhTX, due to the lack of
381 NS1 expression (**Fig. 2b-c**). The results further emphasize that the LPhTXdNS1 is
382 ineffective in inhibiting IFNβ promoter activation in immunocompetent MDCK cell lines,
383 causing the virus to be vulnerable to the antiviral activity of IFN that hinders its efficient
384 replication in these immune-competent cell culture models.

385 **Pathogenicity and immunogenicity of LPhTXdNS1**

386 To determine the safety of LPhTXdNS1, female C57BL/6J mice were infected (i.n.)
387 with 10^2-10^4 PFU of LPhTXdNS1. Uninfected mice and mice infected with 10^2 PFU of
388 LPhTX were included as controls. Mice were monitored daily for morbidity and survival
389 up to 14 DPI (**Fig. 3**). Mice infected with 10^2 PFU of LPhTX, where the multibasic cleavage
390 site of HA was removed to a monobasic cleavage site, started losing body weight at 2
391 DPI (**Fig. 3a**) and succumbed to infection by 7 DPI (**Fig. 3b**). However, all mice infected
392 with 10^2, 10^3, or 10^4 PFU of LPhTXdNS1 maintained their initial body weight (**Fig. 3a**) and
393 survived infection during the entire duration of the experiment (**Fig. 3b**). Consistently, viral
394 replication of LPhTXdNS1 was significantly reduced *in vivo* when compared to LPhTX at
395 2 (**Fig. 3c**) and 4 (**Fig. 3d**) DPI in the nasal turbinate (NT) and lung homogenates. Unlike
396 LPhTX, LPhTXdNS1 was not detected in brain tissues of infected mice (**Figs. 3c-d).**

397 To investigate immunogenicity, sera samples from LPhTXdNS1-infected mice were
398 collected weekly for 4 weeks and assessed using HAI assay (**Table 3**). All mice infected
399 with LPhTXdNS1 induced high levels of HAI titers against a highly pathogenic influenza
400 A/Texas/37/2024 H5N1, designated hereafter as HPhTX, indicating its high

401 immunogenicity even after a single dose of infection at lower (10^2 PFU) dose (**Table 3**).
402 Notably, we observed a direct correlation of HAI titers with the amount of LPhTXdNS1
403 used for vaccination.

404 **Histopathology and immunohistochemistry (IHC) of LPhTXdNS1 infected mice**

405 The lung and brain of infected mice were collected for pathological evaluation and
406 quantification of viral antigen (**Fig. 4**). Pathological changes and high percentages of
407 tissue viral antigen (NP) staining were detected in mice infected with 10^2 PFU of LPhTX
408 while mice infected with 10^2 PFU of LPhTXdNS1 lack the presence of viral NP antigen,
409 similar to mock-infected mice (**Figs. 4c-e**). As expected, mock-infected mice did not show
410 any pathological lesions or viral antigen staining in the lungs and brain (**Figs. 4 a-e**). Mice
411 infected with 10^2 PFU of LPhTX showed the highest degree of pathological lesions
412 (moderate to severe, multifocal to coalescing lymphoplasmacytic pneumonia) (**Figs. 4c**
413 **and 5a**) and the highest area of lung staining for viral NP antigen (average percent
414 pathology in the lung was approximately 22% (**Fig. 4c**) and average percentage of lung
415 staining for viral antigen was approximately 19% (**Fig. 4d**)). Histological lesions in the
416 lungs were characterized by multifocal to extensive areas of moderate alveolar damage
417 frequently covered with fibrin and moderate infiltration of alveolar septa with lymphocytes,
418 plasma cells and macrophages (**Figs. 4a and 5a**). Viral antigen staining was strongest in
419 the bronchial epithelial cells that extended to surrounding alveolar epithelium and
420 occasional nuclear staining of the cell in the alveolar septa (**Figs. 4b and 5b**). The
421 average percent pathology in the lung was approximately ≤1%, and the average
422 percentage of lung staining for viral NP antigen was approximately 5%, 0.7% and 0.1%
423 for mice infected with 10^4 PFU, 10^3 PFU and 10^2 PFU of LPhTXdNS1, respectively (**Figs.**
424 **4c-e**). No lesions in the brain were found in any of the LPhTXdNS1-infected mice, or
425 LPhTX (**Figs. 4a and 5a**).

426 **LPhTXdNS1 vaccination protects against a lethal challenge with H5N1**

427 Since infection with LPhTXdNS1 was not lethal in mice and was associated with
428 seroconversion, we challenged LPhTXdNS1-infected mice with a lethal dose (10^3 PFU)
429 of a recombinant A/Texas/37/2024 H5N1 expressing nanoluciferase (Nluc), designated
430 hereafter as HPhTX-Nluc (**Fig. 6**). As expected, mock-vaccinated mice challenge with
431 HPhTX-Nluc lost body weight starting at 2 days post-challenge (**Fig. 6a**), and all of them

432 succumbed to infection by days 6 and 7 after challenge (**Fig. 6b**). In contrast, all mice
433 vaccinated with LPhTXdNS1 showed no reduction in body weight and all mice survived
434 the lethal challenge with HPhTX-Nluc, except one mouse vaccinated with the lower dose
435 of 10^2 PFU of LPhTXdNS1 that succumbed to infection with HPhTX-Nluc at day 9 after
436 challenge (**Figs. 6a** and **6b**). The presence of HPhTX-Nluc challenge virus in animals
437 used to measure body weight changes and survival was detected using a non-invasive *in*
438 *vivo* imaging system (IVIS). Strong Nluc signal in the lungs of mock-vaccinated mice was
439 detected at days 4 and 6 post-challenge with HPhTX-Nluc (**Fig. 6c**), whereas no Nluc
440 signal was detected in mice vaccinated with LPhTXdNS1, except in one mouse that was
441 vaccinated with a lower dose of 10^2 PFU of LPhTXdNS1 (**Fig. 6c**), that correspond to the
442 mouse that did not survived challenge with HPhTX-Nluc (**Fig. 6b**). The serum samples
443 for this mouse showed a reduced HAI titers when compared to other counterparts
444 vaccinated with the same dose for up to 4 weeks post-infection (**Table 3**).

445 Consistently, in the necropsy mice groups, strong Nluc signal was detected in the
446 lungs of mock-vaccinated mice at days 4 and 6 post-challenge with HPhTX-Nluc (**Fig.**
447 **6d**), whereas no Nluc signal was detected in LPhTXdNS1-vaccinated mice (**Fig. 6d**). All
448 vaccinated mice groups, including those with the lower dose (10^2 PFU) of LPhTXdNS1
449 did not show Nluc signal in the lungs or brains (**Fig. 6d**). Notably, we were able to detect
450 Nluc signal in the brain of mock-vaccinated mice after challenge with HPhTX-Nluc at day
451 6 post-infection, although only in 2 of the challenged animals (**Fig. 6d**). The protection
452 efficacy of LPhTXdNS1 was also confirmed by assessing viral titers of HPhTX-Nluc in the
453 NT, lungs, and brains of vaccinated animals by viral titration, and Nluc expression (**Fig.**
454 **7**). As expected, we detected high viral titers of HPhTX-Nluc in mock-vaccinated mice as
455 determined by Nluc expression (**Figs. 7a and 7c**) and viral titration (**Figs. 7b and 7d**) at
456 4 (**Figs. 7a and 7b**) and 6 (**Figs. 7c and 7d**) days post-challenge with HPhTX-Nluc.
457 These *in vivo* results indicate the high protection efficacy of LPhTXdNS1 against HPhTX.

458 **Histopathology and IHC of mice vaccinated with LPhTXdNS1 following challenge**
459 **with HPhTX-Nluc**

460 The protective efficacy of LPhTXdNS1 was further confirmed by evaluating
461 histopathological lesions and the presence of viral NP antigen in the lung and brain
462 tissues of vaccinated mice after challenge with HPhTX-Nluc (**Fig. 8**). **Figures 8a and 8b**

463 represent the H&E and IHC stained brain and lung tissues of all mice included in the
464 study, respectively. **Figures 9a and 9b** show the H&E and IHC stained brain and lung of
465 representative mice at higher magnifications**.** HPhTX-Nluc- challenged, mock vaccinated,
466 mice showed the most severe pathological lesions, that were similar to those seen in
467 animals infected with 10^2 PFU of LPhTX, consisting of moderate to severe, multifocal to
468 coalescing lymphoplasmacytic pneumonia (**Figs. 8a and 9a**). The average percent
469 pathology in the lung was approximately 37% (**Fig. 8c**) and average percentage of lung
470 staining for viral antigen was 7% (**Fig. 8d**). One mouse in this group showed multifocal,
471 mild perivascular cuffing of lymphocytes in the mid brain (**Fig. 9a**, mild multifocal
472 lymphoplasmacytic encephalitis). LPhTXdNS1-vaccinated mice challenged with HPhTX-
473 Nluc showed mild to minimal pathological lesions. The lesions and IHC pattern were
474 comparable to those in mock-infected mice (**Fig. 9a**). The average percent pathology in
475 the lung was ≤1% and average percentage of lung staining for viral antigen was ≤1% for
476 all vaccinated mice with the different doses of LPhTXdNS1, respectively. There were
477 multifocal areas of viral NP staining in the mid brain and brain stem regions
478 (approximately 3%) (**Figs. 8e and 9b**) and scattered viral NP staining in bronchial
479 epithelial cells and in the alveolar septa of infected mock-vaccinated mice (**Figs. 9a and**
480 **9b**). The vaccinated groups showed rare viral NP staining in the bronchial epithelial cells
481 and alveolar septa. No viral NP antigen was detected in the brain of LPhTXdNS1-
482 vaccinated, HPhTX-Nluc-challenged groups (**Fig. 9b**).
483

484 **Discussion**

485 Influenza is one of the most significant respiratory viral pathogens, responsible for
486 about 2% of all annual respiratory deaths (42). It predominantly affects high-risk groups,
487 including children, the elderly, pregnant women, and immunocompromised individuals
488 (43). Vaccination is the most effective methods for preventing influenza disease,
489 especially in high-risk groups (43). Along with inactivated influenza vaccines, LAIVs play
490 a crucial role in preventing seasonal IAV infections. LAIVs offer the advantages of needle-
491 free administration, the ability to stimulate mucosal immune responses, and are approved
492 for use in healthy individuals aged 2 to 49 years (8, 44).

493 The currently approved LAIV is based on a genetically modified, *ts*, *ca*, *att* influenza
494 strain derived from A/Ann Arbor/6/1960 H2N2 with restricted ability to replicate in the
495 upper (33°C) rather than lower (37°C) respiratory tract, preventing disease onset. LAIV
496 mimics a natural infection, offering the advantage of stimulating mucosal, cellular, and
497 cross-protective immune responses. Despite these advantages, the effectiveness of the
498 LAIV in many studies is comparable, or even lower, than the inactivated influenza vaccine.
499 Besides, the possible reversion of the changes that are responsible for the ts, ca, att of
500 the current form of LAIV due to the evolutionary process may enhance virus replication
501 (45). Unexpected replication of the vaccine virus and reversion to pathogenic strains in
502 immunocompromised patients has been documented for other attenuated vaccine strains
503 (46-48). Therefore, certain key populations are excluded from LAIV recommendations.
504 The current outbreak of HPAIV H5N1 clade 2.3.4.4.b, genotype B3.13, among dairy
505 cattle was first identified in the US in March 2024 (1). In parallel, the genotype D1.1, a
506 reassortant of genotype A3, could quickly spread to all North American flyways and
507 became the predominant genotype in migratory birds, and was recently also documented
508 in dairy cattle in Nevada with adaptive D701N and E627K markers of mammalian host
509 adaptation (3). Human cases of HPAIV H5N1 among dairy farm workers started to be
510 reported in April 2024 in Texas. Cumulatively, 70 confirmed HPAIV H5N1 cases (clade
511 2.3.4.4b, genotypes B3.13 and D1.1) have been documented including one fatality (49).
512 While the current public health risk remains low, these findings have increased the
513 potential for exposure to the virus among individuals working with infected poultry and
514 cattle, such as farm and dairy workers and veterinarians. As a result, the development of
515 an effective HPAIV H5N1 2.3.4.4b vaccine has become essential to protect these high-
516 risk groups.
517 In this study, we developed an efficient and safe live-attenuated dNS1-based 2.3.4.4b
518 H5N1 candidate vaccine with high immunogenicity and efficacy in mice. Unlike the
519 currently in-use LAIVs, which incorporate changes to make the vaccine strain ts (50), the
520 complete deletion of the NS1 protein ensures that the virus is unlikely to restore
521 pathogenicity after successive passaging (51). Several studies have explored the use of
522 truncated or deleted NS1 as a safe vaccination platform against various IAVs, including
523 those affecting avian (52), swine (53), canine (54), equine (55), and humans (22, 56), as

524 well as H5N1 (57), demonstrating its high safety profile. Moreover, a recent study
525 suggested a mechanism to minimize the risk of the current LAIV by applying a targeted
526 approach to mutate the NS1 protein of the LAIV backbone making it unable to bind the
527 host factor CPSF30 (58), allowing the processing of host pre-mRNAs, including those for
528 IFN (21). Consistently, in this work, infections with the highly pathogenic (HPhTX) and low
529 pathogenic (LPhTX) strains with intact NS1 were associated with systemic infection,
530 including neurovirulence in the case of HPhTX (25), while infection with LPhTXdNS1 did
531 not result in systemic infection and/or neurotropism. This emphasizes that LPhTXdNS1
532 could be a safer option as a LAIV.

533 One potential concern with using LPhTXdNS1 is the risk of reassortment with other
534 IAV that may naturally infect the vaccinated individual, potentially leading to the
535 emergence of new virus reassortants. However, reassortment typically occurs when two
536 IAVs with efficient replication co-infect the same host cell (59). The deletion of NS1 in
537 H5N1 viruses typically leads to a virus that induces a stronger innate immune response,
538 which can restrict its ability to replicate efficiently, or block the infection of other influenza
539 strains that are sensitive to IFN. This reduces the severity of the infection and make the
540 virus less capable of spreading in the host (60). It is also important to note that
541 LPhTXdNS1 exhibits reduced replication efficiency in standard immunocompetent
542 mammalian cells, and it has limited replication outside IFN-deficient Vero cells, which are
543 recommended for growing IFN-sensitive viruses, including IAV lacking NS1. These
544 characteristics reduce the likelihood of reassortment of LPhTXdNS1 with other IAVs.

545 Taken together, we have developed LPhTXdNS1 and demonstrated its potential as a
546 safe, immunogenic, and effective vaccine against the recently emerged 2.3.4.4b H5N1.
547 This work serves as a proof-of-concept study for the development of a universal avian
548 influenza vaccine targeting currently emerging strains with potential zoonotic risks. We
549 propose that further studies are needed to evaluate the impact of a multidose LAIV
550 approach and to investigate the vaccine's efficacy in animals, including those currently
551 susceptible to HPAIV infections where the LPhTXdNS1 vaccine could be used (poultry
552 and farm animals). Our approach offers the potential to expand the applications of the
553 current LAIV, particularly in targeting high-risk populations where the burden of IAV
554 remains a significant concern.

Acknowledgments

We thank the Histology unit team staff, Dr. Renee Escalona and Mr. Colin Chuba, for their assistance in tissue staining/immunostaining experiments, and the Cell Biology Core Lab at Texas Biomedical Research Institute for assistance with the multiplex cytokine assay. We also acknowledge the BEI Resources for providing the PB1 (Clone F5-46) and PA (Clone 1F6) monoclonal antibodies.

Funding

This work was supported by a grant from the American Lung Association (ALA, to L.M-S) and Texas Biomed Forum (Award # 1520001, to A.M.). Research in L.M-S and A.G.-S. laboratories on influenza were partially funded by the Center for Research on Influenza Pathogenesis and Transmission (CRIPT), one of the National institutes of Health/National Institute of Allergy and Infectious Diseases (NIH/NIAID) funded Centers of Excellence for Influenza Research and Response (CEIRR; contract # 75N93021C00014).

Competing Interest Statement

The A.G.-S. laboratory has received research support from GSK, Pfizer, Senhwa Biosciences, Kenall Manufacturing, Blade Therapeutics, Avimex, Johnson & Johnson, Dynavax, 7Hills Pharma, Pharmamar, ImmunityBio, Accurius, Nanocomposix, Hexamer, N-fold LLC, Model Medicines, Atea Pharma, Applied Biological Laboratories and Merck. A.G.-S. has consulting agreements for the following companies involving cash and/or stock: Castlevax, Amovir, Vivaldi Biosciences, Contrafect, 7Hills Pharma, Avimex, Pagoda, Accurius, Esperovax, Applied Biological Laboratories, Pharmamar, CureLab Oncology, CureLab Veterinary, Synairgen, Paratus, Pfizer and Prosetta. A.G.-S. has been an invited speaker in meeting events organized by Seqirus, Janssen, Abbott, Astrazeneca and NovavaxA.G.-S. is inventor on patents and patent applications on the use of antivirals and vaccines for the treatment and prevention of virus infections and cancer, owned by the Icahn School of Medicine at Mount Sinai, New York. All other authors declare no commercial or financial conflict of interest.

Authors Contributions

Conceptualization: A.M. and L.M-S.; Methodology: A.M., C.Y., R.S.B., V.S., R.M., R.N.P., R.A.E., M.B., E.M.C., N.J., A.C., and A.N.; Data collection and interpretation: A.M., V.S., R.M., T.J.C.A., C.Y., A.G-S., and L.M-S.; Funding acquisition and resources: A.M., T.J.C.A., A.G-S., and L.M-S.; Writing-original draft preparation: A.M. and L.M-S.; Writing-review and editing: all authors have read and agreed to the published version of the manuscript.

Data availability

All data generated or analyzed during this study are included in this published article

References

1. Mostafa A, Naguib Mahmoud M, Nogales A, Barre Ramya S, Stewart James P, García-Sastre A, Martinez-Sobrido L. 2024. Avian influenza A (H5N1) virus in dairy cattle: origin, evolution, and cross-species transmission. mBio 15:e02542-24.
2. CDC. 2025. H5 Bird Flu: Current Situation. https://www.cdc.gov/bird-flu/situation-summary/index.html. Accessed 27/02/2025.
3. USDA. 2025. The Occurrence of Another Highly Pathogenic Avian Influenza (HPAI) Spillover from Wild Birds into Dairy Cattle.
4. Rolfes MA, Flannery B, Chung JR, O'Halloran A, Garg S, Belongia EA, Gaglani M, Zimmerman RK, Jackson ML, Monto AS, Alden NB, Anderson E, Bennett NM, Billing L, Eckel S, Kirley PD, Lynfield R, Monroe ML, Spencer M, Spina N, Talbot HK, Thomas A, Torres SM, Yousey-Hindes K, Singleton JA, Patel M, Reed C, Fry AM, Us Influenza Vaccine Effectiveness Network tIHSN, the Assessment Branch ISDCfDC, Prevention. 2019. Effects of Influenza Vaccination in the United States During the 2017–2018 Influenza Season. Clinical Infectious Diseases 69:1845-1853.
5. Frutos AM, Price AM, Harker E, Reeves EL, Ahmad HM, Murugan V, Martin ET, House S, Saade EA, Zimmerman RK, Gaglani M, Wernli KJ, Walter EB, Michaels MG, Staat MA, Weinberg GA, Selvarangan R, Boom JA, Klein EJ, Halasa NB, Ginde AA, Gibbs KW, Zhu Y, Self WH, Tartof SY, Klein NP, Dascomb K, DeSilva MB, Weber ZA, Yang DH, Ball SW, Surie D, DeCuir J, Dawood FS, Moline HL, Toepfer AP, Clopper BR, Link-Gelles R, Payne AB, Chung JR, Flannery B, Lewis NM, Olson SM, Adams K, Tenforde MW, Garg S, Grohskopf LA, Reed C, Ellington S. 2024. Interim Estimates of 2023-24 Seasonal Influenza Vaccine Effectiveness - United States. MMWR Morb Mortal Wkly Rep 73:168-174.
6. Zeno EE, Nogareda F, Regan A, Couto P, Rondy M, Jara J, Voto C, Rojas Mena MP, Katz N, Del Valle Juarez M, Benedetti E, de Paula Júnior FJ, Ferreira da Almeida WA, Hott CE, Ferrari PR, Mallegas NV, Vigueras MA, Domínguez C, von Horoch M, Vazquez C, Silvera E, Chiparelli H, Goni N, Castro L, Marcenac P, Kondor RJ, Leite J, Velandia M, Azziz-Baumgartner E, Fowlkes AL, Salas D. Interim Effectiveness

Estimates of 2024 Southern Hemisphere Influenza Vaccines in Preventing Influenza-Associated Hospitalization - REVELAC-i Network, Five South American Countries, March-July 2024. 73(39):861-868.

7. Grohskopf LA, Ferdinands JM, Blanton LH, Broder KR, Loehr J. 2024. Prevention and Control of Seasonal Influenza with Vaccines: Recommendations of the Advisory Committee on Immunization Practices - United States, 2024-25 Influenza Season. MMWR Recomm Rep 73:1-25.
8. Rathnasinghe R, Chang LA, Pearl R, Jangra S, Aspelund A, Hoag A, Yildiz S, Mena I, Sun W, Loganathan M, Crossland NA, Gertje HP, Tseng AE, Aslam S, Albrecht RA, Palese P, Krammer F, Schotsaert M, Muster T, García-Sastre A. 2024. Sequential immunization with chimeric hemagglutinin ΔNS1 attenuated influenza vaccines induces broad humoral and cellular immunity. NPJ Vaccines 9:169.
9. Sanz-Muñoz I, Sánchez-Martínez J, Rodríguez-Crespo C, Concha-Santos Corina S, Hernández M, Rojo-Rello S, Domínguez-Gil M, Mostafa A, Martinez-Sobrido L, Eiros Jose M, Nogales A. 2024. Are we serologically prepared against an avian influenza pandemic and could seasonal flu vaccines help us? mBio 16:e03721-24.
10. Ichinohe T, Tamura S, Kawaguchi A, Ninomiya A, Imai M, Itamura S, Odagiri T, Tashiro M, Takahashi H, Sawa H, Mitchell WM, Strayer DR, Carter WA, Chiba J, Kurata T, Sata T, Hasegawa H. 2007. Cross-protection against H5N1 influenza virus infection is afforded by intranasal inoculation with seasonal trivalent inactivated influenza vaccine. J Infect Dis 196:1313-20.
11. Matrajt L, Halloran ME, Antia R. 2020. Successes and Failures of the Live-attenuated Influenza Vaccine: Can We Do Better? Clin Infect Dis 70:1029-1037.
12. Si L, Shen Q, Li J, Chen L, Shen J, Xiao X, Bai H, Feng T, Ye AY, Li L, Zhang C, Li Z, Wang P, Oh CY, Nurani A, Niu S, Zhang C, Wei X, Yuan W, Liao H, Huang X, Wang N, Tian W-x, Tian H, Li L, Liu X, Plebani R. 2022. Generation of a live attenuated influenza A vaccine by proteolysis targeting. Nature Biotechnology 40:1370-1377.
13. Smith A, Rodriguez L, El Ghouayel M, Nogales A, Chamberlain JM, Sortino K, Reilly E, Feng C, Topham DJ, Martínez-Sobrido L, Dewhurst S. 2020. A Live Attenuated Influenza Vaccine Elicits Enhanced Heterologous Protection When the Internal Genes of the Vaccine Are Matched to Those of the Challenge Virus. J Virol 94.
14. Kildegaard H, Lund LC, Pottegård A, Stensballe LG. 2023. Effectiveness of the quadrivalent live attenuated influenza vaccine against influenza-related hospitalisations and morbidity among children aged 2 to 6 years in Denmark: a nationwide cohort study emulating a target trial. The Lancet Child & Adolescent Health 7:852-862.
15. Nolan T, Richmond PC, Formica NT, Höschler K, Skeljo MV, Stoney T, McVernon J, Hartel G, Sawlwin DC, Bennet J, Ryan D, Basser RL, Zambon MC. 2008. Safety and immunogenicity of a prototype adjuvanted inactivated split-virus influenza A (H5N1) vaccine in infants and children. Vaccine 26:6383-91.
16. Chotpitayasunondh T, Thisyakorn U, Pancharoen C, Pepin S, Nougarede N. 2008. Safety, humoral and cell mediated immune responses to two formulations of an inactivated, split-virion influenza A/H5N1 vaccine in children. PLoS One 3:e4028.

17. Gouma S, Anderson EM, Hensley SE. 2020. Challenges of Making Effective Influenza Vaccines. Annu Rev Virol 7:495-512.
18. Krammer F, Palese P. 2015. Advances in the development of influenza virus vaccines. Nat Rev Drug Discov 14:167-82.
19. Petersen H, Mostafa A, Tantawy MA, Iqbal AA, Hoffmann D, Tallam A, Selvakumar B, Pessler F, Beer M, Rautenschlein S, Pleschka S. 2018. NS Segment of a 1918 Influenza A Virus-Descendent Enhances Replication of H1N1pdm09 and Virus-Induced Cellular Immune Response in Mammalian and Avian Systems. Front Microbiol 9:526.
20. Kanrai P, Mostafa A, Madhugiri R, Lechner M, Wilk E, Schughart K, Ylösmäki L, Saksela K, Ziebuhr J, Pleschka S. 2016. Identification of specific residues in avian influenza A virus NS1 that enhance viral replication and pathogenicity in mammalian systems. Journal of General Virology 97:2135-2148.
21. Khalil AM, Nogales A, Martínez-Sobrido L, Mostafa A. 2024. Antiviral responses versus virus-induced cellular shutoff: a game of thrones between influenza A virus NS1 and SARS-CoV-2 Nsp1. Frontiers in Cellular and Infection Microbiology 14.
22. Wang P, Zheng M, Lau S-Y, Chen P, Mok Bobo W-Y, Liu S, Liu H, Huang X, Cremin Conor J, Song W, Chen Y, Wong Y-C, Huang H, To Kelvin K-W, Chen Z, Xia N, Yuen K-Y, Chen H. 2019. Generation of DelNS1 Influenza Viruses: a Strategy for Optimizing Live Attenuated Influenza Vaccines. mBio 10:10.1128/mbio.02180-19.
23. Nogales A, DeDiego ML, Martínez-Sobrido L. 2022. Live attenuated influenza A virus vaccines with modified NS1 proteins for veterinary use. Front Cell Infect Microbiol 12:954811.
24. Hai R, Martínez-Sobrido L, Fraser KA, Ayllon J, García-Sastre A, Palese P. 2008. Influenza B virus NS1-truncated mutants: live-attenuated vaccine approach. J Virol 82:10580-90.
25. Mostafa A, Barre RS, Allué-Guardia A, Escobedo RA, Shivanna V, Rothan H, Castro EM, Ma Y, Cupic A, Jackson N, Bayoumi M, Torrelles JB, Ye C, García-Sastre A, Martinez-Sobrido L. 2025. Replication kinetics, pathogenicity and virus-induced cellular responses of cattle-origin influenza A(H5N1) isolates from Texas, United States. Emerging Microbes & Infections 14:2447614.
26. Steinig E, Coin LJJoOSS. 2022. Nanoq: ultra-fast quality control for nanopore reads. 7:2991.
27. Salmela L, Walve R, Rivals E, Ukkonen E. 2017. Accurate self-correction of errors in long reads using de Bruijn graphs. Bioinformatics 33:799-806.
28. Li H. 2016. Minimap and miniasm: fast mapping and de novo assembly for noisy long sequences. Bioinformatics 32:2103-10.
29. Li H, Handsaker B, Wysoker A, Fennell T, Ruan J, Homer N, Marth G, Abecasis G, Durbin R. 2009. The Sequence Alignment/Map format and SAMtools. Bioinformatics 25:2078-9.
30. Pedersen BS, Quinlan AR. 2018. Mosdepth: quick coverage calculation for genomes and exomes. Bioinformatics 34:867-868.
31. Wilm A, Aw PP, Bertrand D, Yeo GH, Ong SH, Wong CH, Khor CC, Petric R, Hibberd ML, Nagarajan N. 2012. LoFreq: a sequence-quality aware, ultra-sensitive variant

712 caller for uncovering cell-population heterogeneity from high-throughput
713 sequencing datasets. Nucleic Acids Res 40:11189-201.
714 32. Nogales A, Baker SF, Martínez-Sobrido L. 2015. Replication-competent influenza A
715 viruses expressing a red fluorescent protein. Virology 476:206-216.
716 33. Nogales A, Rodríguez-Sánchez I, Monte K, Lenschow DJ, Perez DR, Martínez-Sobrido
717 L. 2016. Replication-competent fluorescent-expressing influenza B virus. Virus Res
718 213:69-81.
719 34. Martínez-Sobrido L, García-Sastre A. 2010. Generation of recombinant influenza
720 virus from plasmid DNA. J Vis Exp doi:10.3791/2057.
721 35. Mostafa A, Kanrai P, Ziebuhr J, Pleschka S. 2013. Improved dual promotor-driven
722 reverse genetics system for influenza viruses. J Virol Methods 193:603-10.
723 36. Mostafa A, Kanrai P, Petersen H, Ibrahim S, Rautenschlein S, Pleschka S. 2015.
724 Efficient Generation of Recombinant Influenza A Viruses Employing a New
725 Approach to Overcome the Genetic Instability of HA Segments. PLOS ONE
726 10:e0116917.
727 37. Mostafa A, Kanrai P, Ziebuhr J, Pleschka S. 2016. The PB1 segment of an influenza A
728 virus H1N1 2009pdm isolate enhances the replication efficiency of specific
729 influenza vaccine strains in cell culture and embryonated eggs. J Gen Virol 97:620-
730 631.
731 38. O'Neill RE, Talon J, Palese P. 1998. The influenza virus NEP (NS2 protein) mediates
732 the nuclear export of viral ribonucleoproteins. Embo j 17:288-96.
733 39. Chiem K, Nogales A, Martinez-Sobrido L. 2022. Generation, Characterization, and
734 Applications of Influenza A Reporter Viruses. Methods Mol Biol 2524:249-268.
735 40. Grodeland G, Mjaaland S, Roux KH, Fredriksen AB, Bogen B. 2013. DNA Vaccine that
736 Targets Hemagglutinin to MHC Class II Molecules Rapidly Induces Antibody-
737 Mediated Protection against Influenza. The Journal of Immunology 191:3221-3231.
738 41. Delahaye C, Nicolas J. 2021. Sequencing DNA with nanopores: Troubles and biases.
739 PLoS One 16:e0257521.
740 42. Paget J, Spreeuwenberg P, Charu V, Taylor RJ, Iuliano AD, Bresee J, Simonsen L,
741 Viboud C. 2019. Global mortality associated with seasonal influenza epidemics:
742 New burden estimates and predictors from the GLaMOR Project. J Glob Health
743 9:020421.
744 43. Antonelli Incalzi R, Consoli A, Lopalco P, Maggi S, Sesti G, Veronese N, Volpe M.
745 2024. Influenza vaccination for elderly, vulnerable and high-risk subjects: a narrative
746 review and expert opinion. Internal and Emergency Medicine 19:619-640.
747 44. Calzas C, Chevalier C. 2019. Innovative Mucosal Vaccine Formulations Against
748 Influenza A Virus Infections. Front Immunol 10:1605.
749 45. Zhou B, Meliopoulos VA, Wang W, Lin X, Stucker KM, Halpin RA, Stockwell TB,
750 Schultz-Cherry S, Wentworth DE. 2016. Reversion of Cold-Adapted Live Attenuated
751 Influenza Vaccine into a Pathogenic Virus. J Virol 90:8454-63.
752 46. Banovic T, Yanilla M, Simmons R, Robertson I, Schroder WA, Raffelt NC, Wilson YA,
753 Hill GR, Hogan P, Nourse CB. 2011. Disseminated varicella infection caused by
754 varicella vaccine strain in a child with low invariant natural killer T cells and
755 diminished CD1d expression. J Infect Dis 204:1893-901.

47. WHO. 2017. Poliomyelitis: Vaccine derived polio.
48. Bull JJ. 2015. Evolutionary reversion of live viral vaccines: Can genetic engineering subdue it? Virus Evol 1.
49. CDC. 2025. H5 Bird Flu: Current Situation. https://www.cdc.gov/bird-flu/situation-summary/index.html. Accessed 02.18.2025.
50. Zhou B, Li Y, Speer SD, Subba A, Lin X, Wentworth DE. 2012. Engineering temperature sensitive live attenuated influenza vaccines from emerging viruses. Vaccine 30:3691-702.
51. Zhou B, Meliopoulos Victoria A, Wang W, Lin X, Stucker Karla M, Halpin Rebecca A, Stockwell Timothy B, Schultz-Cherry S, Wentworth David E. 2016. Reversion of Cold-Adapted Live Attenuated Influenza Vaccine into a Pathogenic Virus. Journal of Virology 90:8454-8463.
52. Wang L, Suarez DL, Pantin-Jackwood M, Mibayashi M, García-Sastre A, Saif YM, Lee CW. 2008. Characterization of influenza virus variants with different sizes of the non-structural (NS) genes and their potential as a live influenza vaccine in poultry. Vaccine 26:3580-3586.
53. Vandoorn E, Stadejek W, Parys A, Chepkwony S, Chiers K, Van Reeth K. 2022. Pathobiology of an NS1-Truncated H3N2 Swine Influenza Virus Strain in Pigs. Journal of Virology 96:e00519-22.
54. Nogales A, Huang K, Chauché C, DeDiego ML, Murcia PR, Parrish CR, Martínez-Sobrido L. 2017. Canine influenza viruses with modified NS1 proteins for the development of live-attenuated vaccines. Virology 500:1-10.
55. Quinlivan M, Zamarin D, García-Sastre A, Cullinane A, Chambers T, Palese P. 2005. Attenuation of equine influenza viruses through truncations of the NS1 protein. J Virol 79:8431-9.
56. Talon J, Salvatore M, O'Neill RE, Nakaya Y, Zheng H, Muster T, García-Sastre A, Palese P. 2000. Influenza A and B viruses expressing altered NS1 proteins: A vaccine approach. Proceedings of the National Academy of Sciences 97:4309-4314.
57. Steel J, Lowen Anice C, Pena L, Angel M, Solórzano A, Albrecht R, Perez Daniel R, García-Sastre A, Palese P. 2009. Live Attenuated Influenza Viruses Containing NS1 Truncations as Vaccine Candidates against H5N1 Highly Pathogenic Avian Influenza. Journal of Virology 83:1742-1753.
58. Bonifacio J, Williams N, Garnier L, Hugues S, Schmolke M, Mazel-Sanchez B. 2022. Optimizing the Live Attenuated Influenza A Vaccine Backbone for High-Risk Patient Groups. J Virol 96:e0087122.
59. Phipps KL, Marshall N, Tao H, Danzy S, Onuoha N, Steel J, Lowen AC. 2017. Seasonal H3N2 and 2009 Pandemic H1N1 Influenza A Viruses Reassort Efficiently but Produce Attenuated Progeny. Journal of Virology 91:10.1128/jvi.00830-17.
60. Nogales A, Schotsaert M, Rathnasinghe R, DeDiego ML, García-Sastre A, Martinez-Sobrido L. 2021. Replication-Competent ΔNS1 Influenza A Viruses Expressing Reporter Genes. Viruses 13.

Tables

Table 1. Data description - Sample summary and genome coverage

Sample	n Reads	n50	Mb	Align. Rate	Mean Coverage	>100x
LPhTX	78,248	1,183	104.1	98.89%	426.6	99.99%
LPhTXdNS1	30,442	1,146	26.7	98.43%	888.5	50.68%

Table 2. Variant frequencies - All variants at <25% allele frequency are shown on the HA and NS segments. Homopolymer indels >3nt have been removed as well.

Virus	Seg.	Pos.	Ref. allele (aa)	Alt. allele (aa)	Alt. freq	Read depth
LPhTX	HA	539	G (Aspartic acid)	A (Asparagine)	41.3%	603
LPhTX	HA	1068	C (Alanine)	T (Valine)	27.2%	1,380
LPhTX	NS	201	C (Arginine)	G (Glycine)	25.7%	966
LPhTX	NS	440	C (Phenylalanine)	G (Leucine)	36.4%	918
LPhTX	NS	444	C (Arginine)	T (Tryptophan)	27.8%	916
LPhTX	NS	445	G (Arginine)	A (Glutamine)	39.2%	921
LPhTXdNS1	HA	539	G (Aspartic acid)	A (Asparagine)	46.5%	863

Table 3. HAI titers against HPhTX in sera from mice immunized with LPhTXdNS1

	HAI titer														
	LPhTXdNS1 10^2 PFU					**LPhTXdNS1 10^3 PFU**					**LPhTXdNS1 10^4 PFU**				
W1	20	10	20	10	10	40	40	20	20	20	80	40	80	20	20
W2	40	40	20	40	20	320	160	160	160	320	80	320	320	160	80
W3	160	80	160	320	80	320	640	320	160	320	320	640	320	640	320
W4	640	160	160	320	40	640	320	320	640	640	320	640	320	640	320

W: week

812 **Figure legends**

813 **Figure 1**. **Generation and characterization of LPhTXdNS1.** (**a**) Schematic
814 representation of influenza low pathogenic human A/Texas/37/2024 H5N1 (LPhTX, left)
815 and NS1 deficient (LPhTXdNS1, right) viruses. Mutation of the multibasic cleavage site of
816 A/Texas/37/2024 H5N1 HA (PLREKRRKR/GLF) to a monobasic cleavage site (PQIETR)
817 that made the backbone of LPhTX and LPhTXdNS1 is indicated on the top right. (**b**)
818 Western blot showing the lack of NS1 protein expression in LPhTXdNS1-infected,
819 compared to LPhTX-infected Vero cells. The PB1, PA, and NP viral proteins were included
820 as viral infection controls. β-actin was included as a loading control. (**c**) Read depth across
821 HA and NS segments – Coverage was calculated across the HA and NS segments for the
822 LPhTX and LPhTXdNS1. The red dotted line represents 100x read depth. The NS gene in
823 LPhTXdNS1 contains a complete NS1 deletion. (**d**) Non-reference allele frequency - The
824 genome of the rescued viruses were compared to the LPhTX reference to identify variant
825 sites. SNV allele frequency from LPhTX and LPhTXdNS1 are shown with circles. Variants
826 on the HA and NS segments are shown in red and blue respectively. Variants <25%
827 frequency and indels caused by homopolymer runs greater than 3 nt are not shown. Allele
828 frequencies are provided in Table 2. The red line indicates 50% allele frequency. (**e**) Plaque
829 phenotypes of LPhTX and LPhTXdNS1 at 33°C (top) and 37°C (bottom) in Vero cells. Both
830 viral stocks were titrated using immunostaining assay 24 hpi. (**f**) Plaque phenotypes of
831 LPhTXdNS1 at 33°C (top) and 37°C (bottom) in MDCK (left) and Vero (right) cells by
832 immunostaining at 48 hpi. (**g**) Growth kinetic of LPhTX and LPhTXdNS1 in Vero cells. Cell
833 monolayers were infected at MOI=0.001 and viral titers at 12, 24, 36 and 48 hpi were
834 determined by plaque assay using an immunostaining assay. A two-way repeated measure
835 ANOVA with Geisser-Greenhouse correction. Post-hoc multiple comparisons performed
836 using Šídák method to compare groups within each time-point. The significant differences
837 are indicated (* = $p < 0.05$, ** = $p < 0.01$, *** = $p < 0.001$).

838 **Figure 2. IFNβ promoter activation by LPhTXdNS1 infection.** (**a**) Schematic
839 representation of the IFNβ induction bioassay: MDCK cells constitutively expressing GFP-
840 CAT and FFluc reporter genes under the control of the IFNβ promoter (MDCK IFNβ GFP-
841 CAT/FFluc) were infected at MOI 2 with LPhTX, LPhTXdNS1, or mock-infected. At 12 hpi,
842 IFNβ promoter activation was determined by GFP (**b**) and FFluc (**c**) expression. The viral

843 NP in infected cells was detected with the HT103 MAb and DAPI was used for nuclear
844 staining. The scale bar was set for 100 μm. BF: Bright-Field; GFP: Green Fluorescent
845 Protein. All data points are shown with black lines representing the mean (n = 3). Groups
846 compared using a Welch's one-way ANOVA, followed by multiple comparisons using
847 Dunnett T3 method (*** = $p < 0.001$; **** = $p < 0.0001$).

848 **Figure 3. Pathogenicity of LPhTXdNS1.** (**a**) Body weight loss of C57BL/6J mice infected
849 with LPhTX (10^2 PFU) or LPhTXdNS1 ($10^{2\text{-}4}$ PFU), control (Ctrl), and mock-infected mice
850 (inoculated with 1XPBS) (n=5). (**b**) Survival rates of C57BL/6J mice in panel a. (**c-d**) Viral
851 replication of LPhTXdNS1 and LPhTX in the nasal turbinate (NT), lung and brain
852 homogenates of mice at 2 (**c**) and 4 (**d**) DPI. Data are presented as mean ± SD. A two-
853 way repeated measure ANOVA with Geisser-Greenhouse correction followed by Dunnett's
854 multiple comparisons test (* = $p < 0.05$, ** = $p < 0.01$, *** = $p < 0.001$).

855 **Figure 4. H&E and IHC staining of lung and brain tissues of mice infected with**
856 **LPhTXdNS1.** (**a**) H&E staining of brain (top) and lung (bottom) tissues of mock-infected
857 and LPhTX- or LPhTXdNS1-infected mice. (**b**) Viral NP antigen IHC staining of brain (top)
858 and lung (bottom) tissues of mock-infected and LPhTX- or LPhTXdNS1-infected mice.
859 Scale bars represent 2 mm. (**c-e**) Quantitative assessment of histologic lesions (**c**) and
860 tissue viral NP antigen positivity (%) in the lung (**d**) and brain (**e**) tissues from mock-
861 infected and LPhTX- and LPhTXdNS1-infected mice. Data are presented as mean ± SD.
862 Differences in quantitative assessment of histologic lesions and percentage of viral
863 antigens were analyzed using beta regression. Post-hoc testing was conducted using
864 Wald's z-test with Tukey's adjustment for multiple comparisons (* = $p < 0.05$;
865 **** = $p < 0.0001$).

866 **Figure 5**. **Histopathological findings in brain and lung sections of mice infected with**
867 **LPhTXdNS1.** H&E staining (**a**) and IHC detection of viral NP antigen (**b**) in the brain (top)
868 and lung (bottom) tissues of mice mock-infected or infected with LPhTX and
869 LPhTXdNS1. First row scale bars of each tissue represent 1000μm and second row scale
870 bars of each tissue represent 100μm. The images displayed at the bottom are directly
871 associated with the corresponding squares shown at the top images.

872 **Figure 6. Protection efficacy of LPhTXdNS1.** (**a**) Body weight loss (%) following
873 vaccination with different doses of LPhTXdNS1 (vLPhTXdNS1) and challenge with 10^3
874 PFU of HPhTX-Nluc. Mock-vaccinated animals challenge with 10^3 PFU of HPhTX-Nluc,
875 and mock-challenged mice, were included as control. (**b**) Survival rate following challenge
876 with HPhTX-Nluc from animals in panel a. (**c**) Nluc expression as determined by IVIS from
877 same group of animals used in panel a to assess morbidity and mortality at 4 and 6 DPI.
878 (**d**) IVIS of necropsy groups of mice and their corresponding lung and brain tissues at 4
879 and 6 DPI.

880 **Figure 7. HPhTX-Nluc viral titers in the NT, lungs, and brains of mice vaccinated with**
881 **LPhTXdNS1.** (**a & b**) Viral replication of HPhTX-Nluc was determined by measuring Nluc
882 activity (**a**) and viral titers (**b**) at day 4 post-challenge. (**c & d**) Viral replication of HPhTX-
883 Nluc was determined by Nluc activity (**c**) and viral titers (**d**) at day 6 post-challenge. Data
884 are presented as mean ± SD. A two-way repeated measure ANOVA with Geisser-
885 Greenhouse correction followed by Dunnett's multiple comparisons test (* = $p < 0.05$,
886 ** = $p < 0.01$, *** = $p < 0.001$, **** = $p < 0.0001$).

887 **Figure 8. Histologic lesions and IHC staining for viral NP antigen after challenge**
888 **with HPhTX-Nluc.** (**a-b**) H&E tissue sections (**a**) and IHC (**b**) of brain (top) and lung
889 (bottom) tissues from mock-vaccinated, mock-challenged mice; mock-vaccinated,
890 challenged mice; and vaccinated mice ($10^{2\text{-}4}$ PFU vLPhTXdNS1), challenge mice. All
891 challenged groups were infected with a lethal infection dose of 10^3 PFU of the HPhTX-
892 Nluc. Scale bars represent 2 mm. (**c-e**) Quantitative assessment of histologic lesions (**c**)
893 and tissue viral NP antigen positivity (%) in the lung (**d**) and brain (**e**) tissues from mice in
894 panel a. Data are presented as mean ± SD. Differences in quantitative assessment of
895 histologic lesions and percentage of viral antigens were analyzed using beta regression.
896 Post-hoc testing was conducted using Wald's z-test with Tukey's adjustment for multiple
897 comparisons (**** = $p < 0.0001$).

898 **Figure 9. Histopathological findings in the brain and lung sections of mice challenge**
899 **with HPhTX-Nluc.** (**a**) H&E staining and (**b**) IHC detection of viral antigen (NP) in in the
900 brain (top) and lung (bottom) tissues. First row scale bars of each tissue represent 1000µm
901 and second row scale bars of each tissue represents 100µm. The images displayed at the
902 bottom are directly associated with the corresponding squares shown at the top images.

Graphical abstract

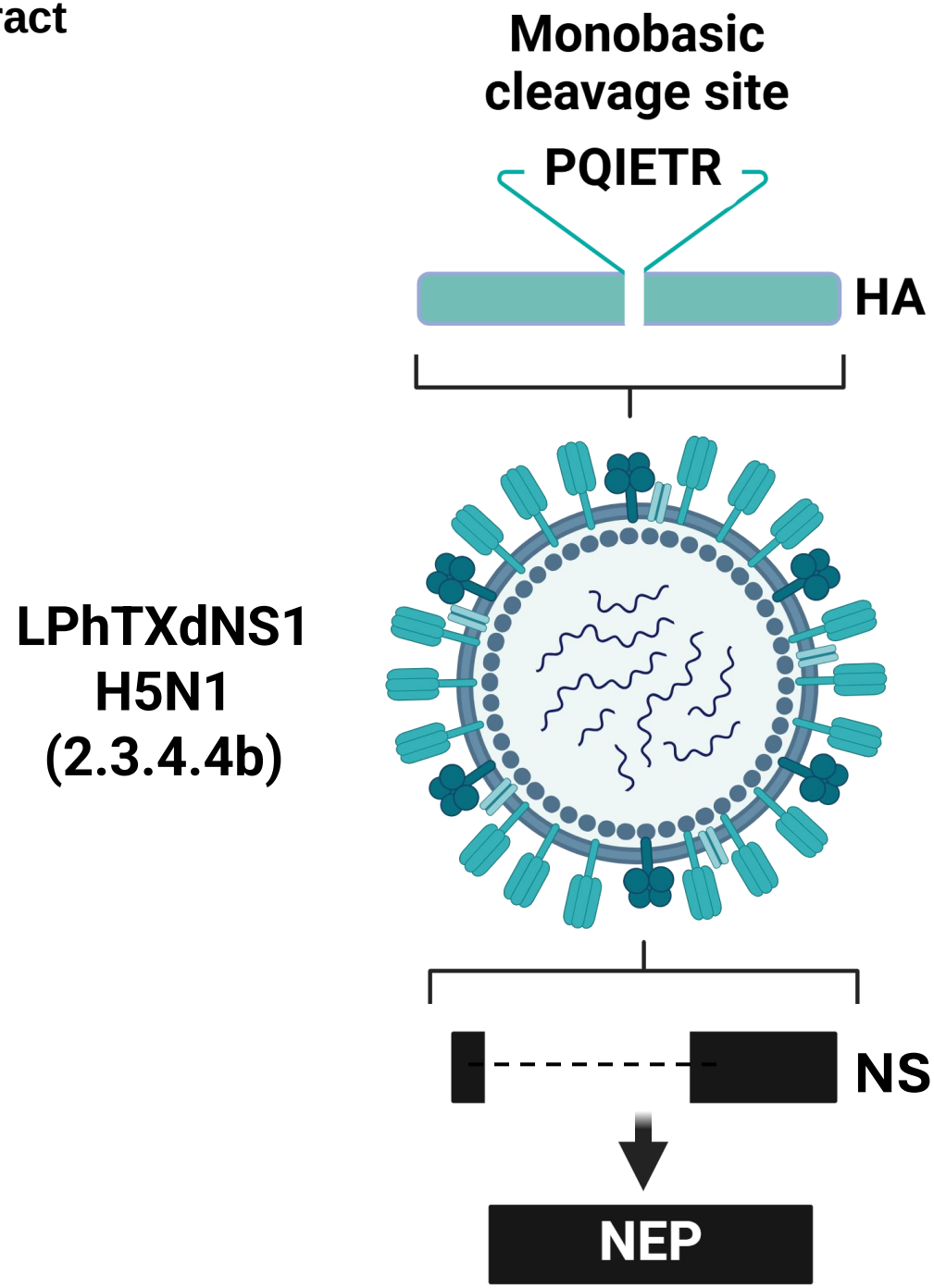

Figure 1

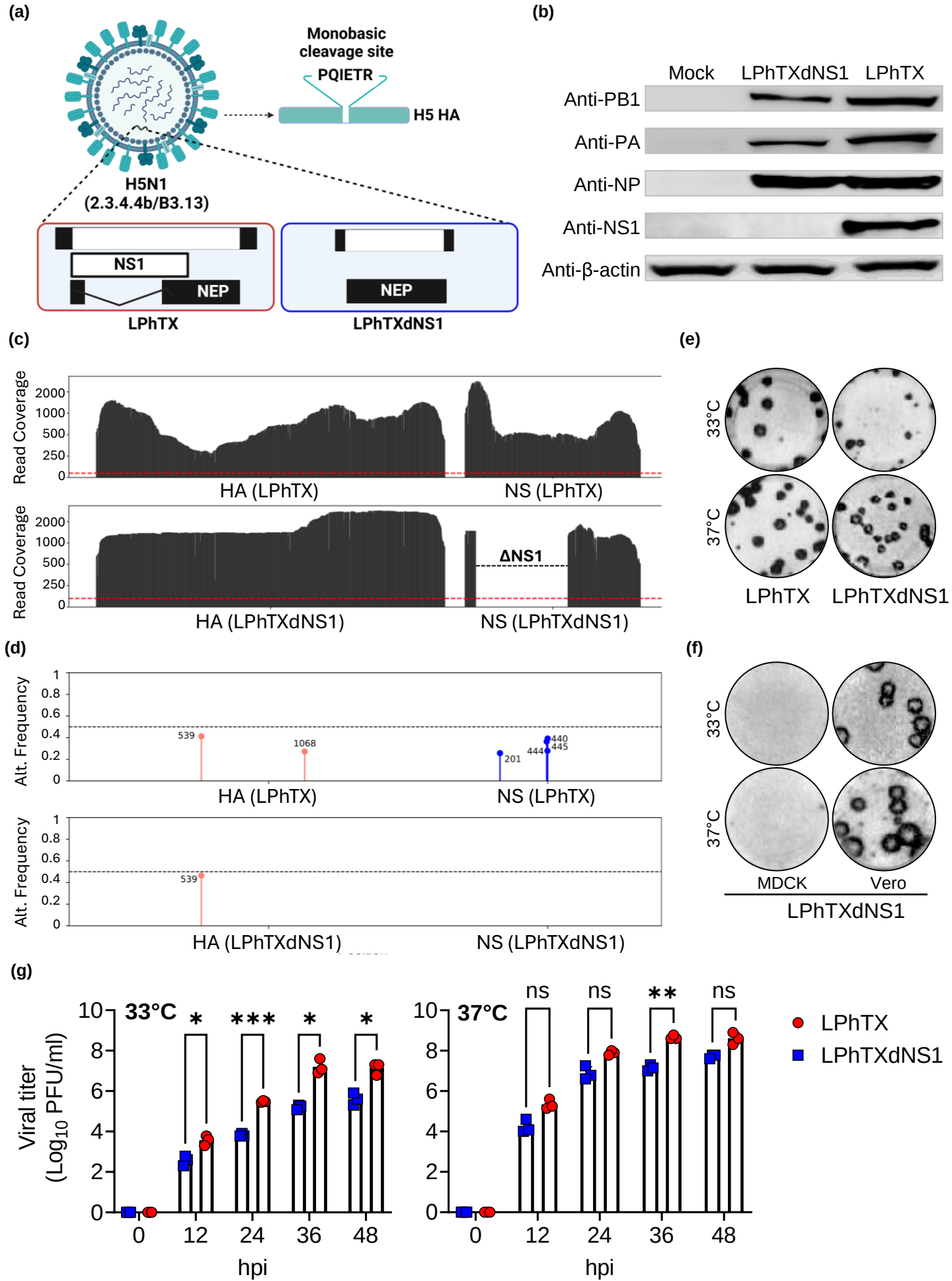
(a)
Monobasic cleavage site
PQIETR
H5 HA
H5N1
(2.3.4.4b/B3.13)
NS1
NEP
LPhTX
NEP
LPhTXdNS1
(b)
Mock
LPhTXdNS1
LPhTX
Anti-PB1
Anti-PA
Anti-NP
Anti-NS1
Anti-β-actin
(c)
Read Coverage
2000
1000
500
250
0
HA (LPhTX)
NS (LPhTX)
ΔNS1
HA (LPhTXdNS1)
NS (LPhTXdNS1)
(d)
Alt. Frequency
1
0.8
0.6
0.4
0.2
0
539
1068
201
444
440
445
HA (LPhTX)
NS (LPhTX)
HA (LPhTXdNS1)
NS (LPhTXdNS1)
(e)
33°C
37°C
LPhTX
LPhTXdNS1
(f)
33°C
37°C
MDCK
Vero
LPhTXdNS1
(g)
33°C
37°C
Viral titer
(Log10 PFU/ml)
10
8
6
4
2
0
*
***
*
*
ns
ns
**
ns
0
12
24
36
48
hpi
LPhTX
LPhTXdNS1

Figure 2

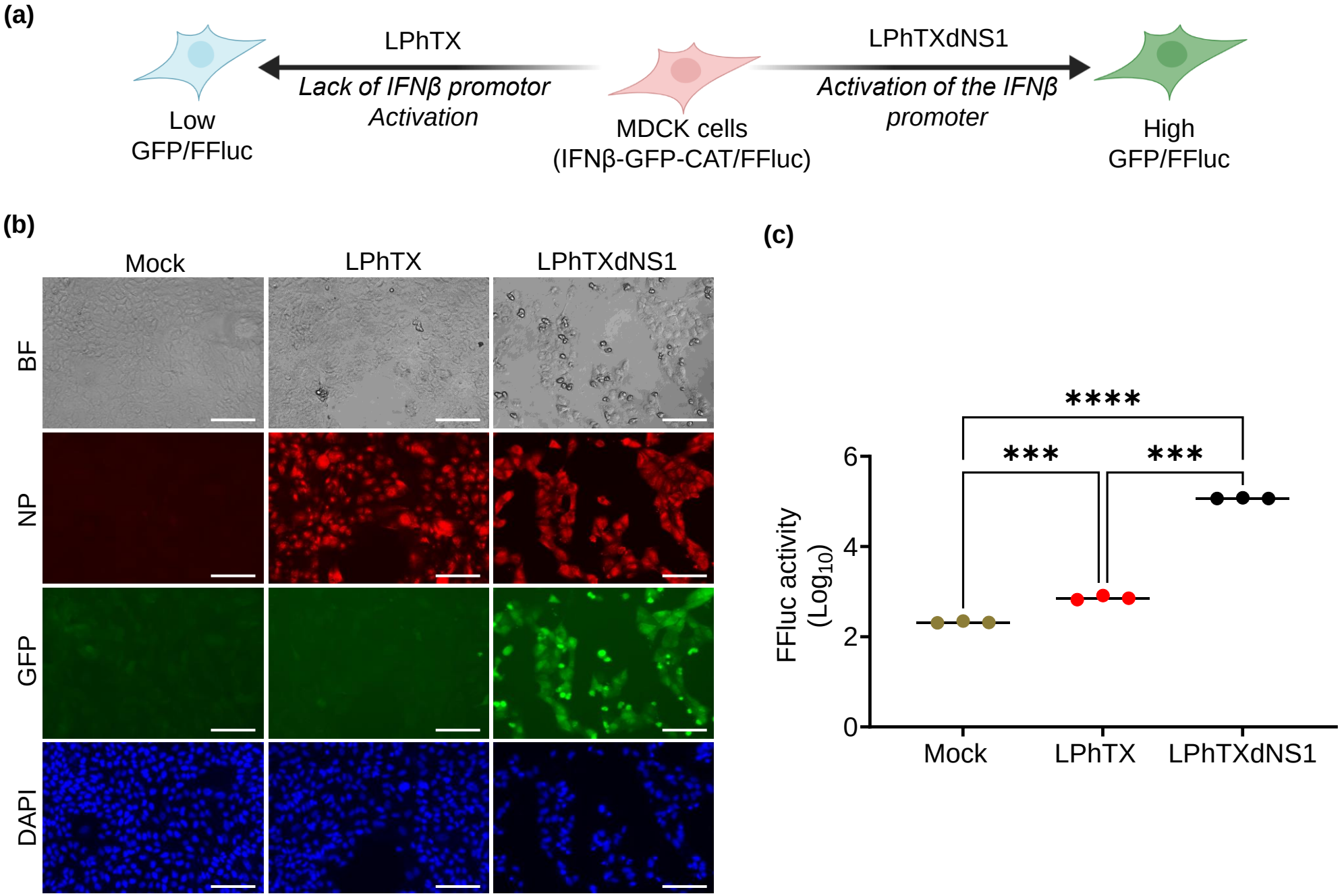
(a)
LPhTX
Lack of IFNβ promotor Activation
Low GFP/FFluc
MDCK cells (IFNβ-GFP-CAT/FFluc)
LPhTXdNS1
Activation of the IFNβ promoter
High GFP/FFluc
(b)
Mock
LPhTX
LPhTXdNS1
BF
NP
GFP
DAPI
(c)
****
***
***
FFluc activity (Log10)
6
4
2
0
Mock
LPhTX
LPhTXdNS1

Figure 3

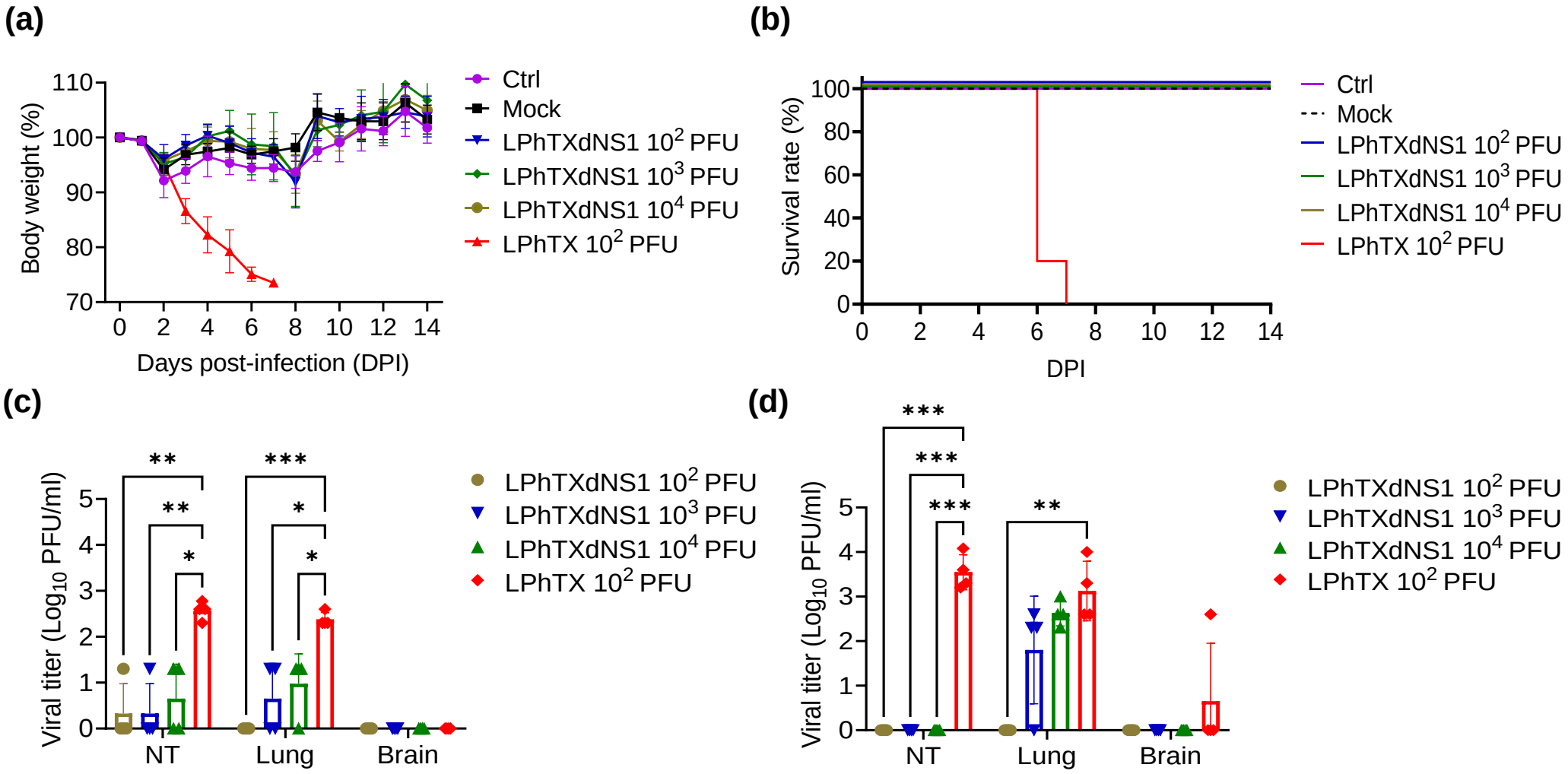
(a)
Body weight (%)
110
100
90
80
70
0 2 4 6 8 10 12 14
Days post-infection (DPI)
Ctrl
Mock
LPhTXdNS1 10^2 PFU
LPhTXdNS1 10^3 PFU
LPhTXdNS1 10^4 PFU
LPhTX 10^2 PFU
(b)
Survival rate (%)
100
80
60
40
20
0
0 2 4 6 8 10 12 14
DPI
Ctrl
Mock
LPhTXdNS1 10^2 PFU
LPhTXdNS1 10^3 PFU
LPhTXdNS1 10^4 PFU
LPhTX 10^2 PFU
(c)
Viral titer (Log10 PFU/ml)
5
4
3
2
1
0
**
**
*
***
*
*
NT
Lung
Brain
LPhTXdNS1 10^2 PFU
LPhTXdNS1 10^3 PFU
LPhTXdNS1 10^4 PFU
LPhTX 10^2 PFU
(d)
Viral titer (Log10 PFU/ml)
5
4
3
2
1
0
***
***
***
**
NT
Lung
Brain
LPhTXdNS1 10^2 PFU
LPhTXdNS1 10^3 PFU
LPhTXdNS1 10^4 PFU
LPhTX 10^2 PFU

Figure 4

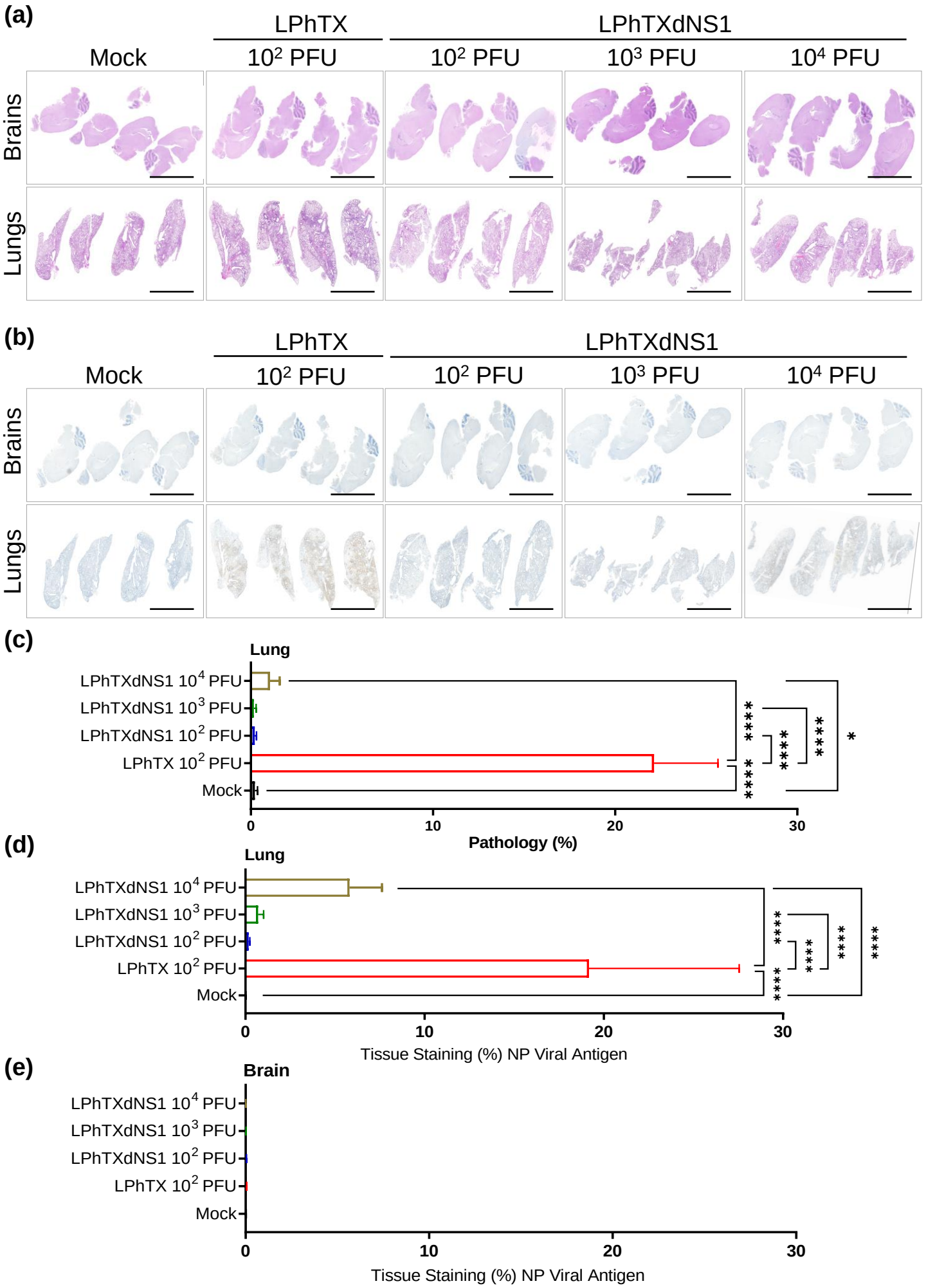
(a)
LPhTX
LPhTXdNS1
Mock
10² PFU
10² PFU
10³ PFU
10⁴ PFU
Brains
Lungs
(b)
LPhTX
LPhTXdNS1
Mock
10² PFU
10² PFU
10³ PFU
10⁴ PFU
Brains
Lungs
(c)
Lung
LPhTXdNS1 10⁴ PFU
LPhTXdNS1 10³ PFU
LPhTXdNS1 10² PFU
LPhTX 10² PFU
Mock
0
10
20
30
Pathology (%)
(d)
Lung
LPhTXdNS1 10⁴ PFU
LPhTXdNS1 10³ PFU
LPhTXdNS1 10² PFU
LPhTX 10² PFU
Mock
0
10
20
30
Tissue Staining (%) NP Viral Antigen
(e)
Brain
LPhTXdNS1 10⁴ PFU
LPhTXdNS1 10³ PFU
LPhTXdNS1 10² PFU
LPhTX 10² PFU
Mock
0
10
20
30
Tissue Staining (%) NP Viral Antigen

Figure 5

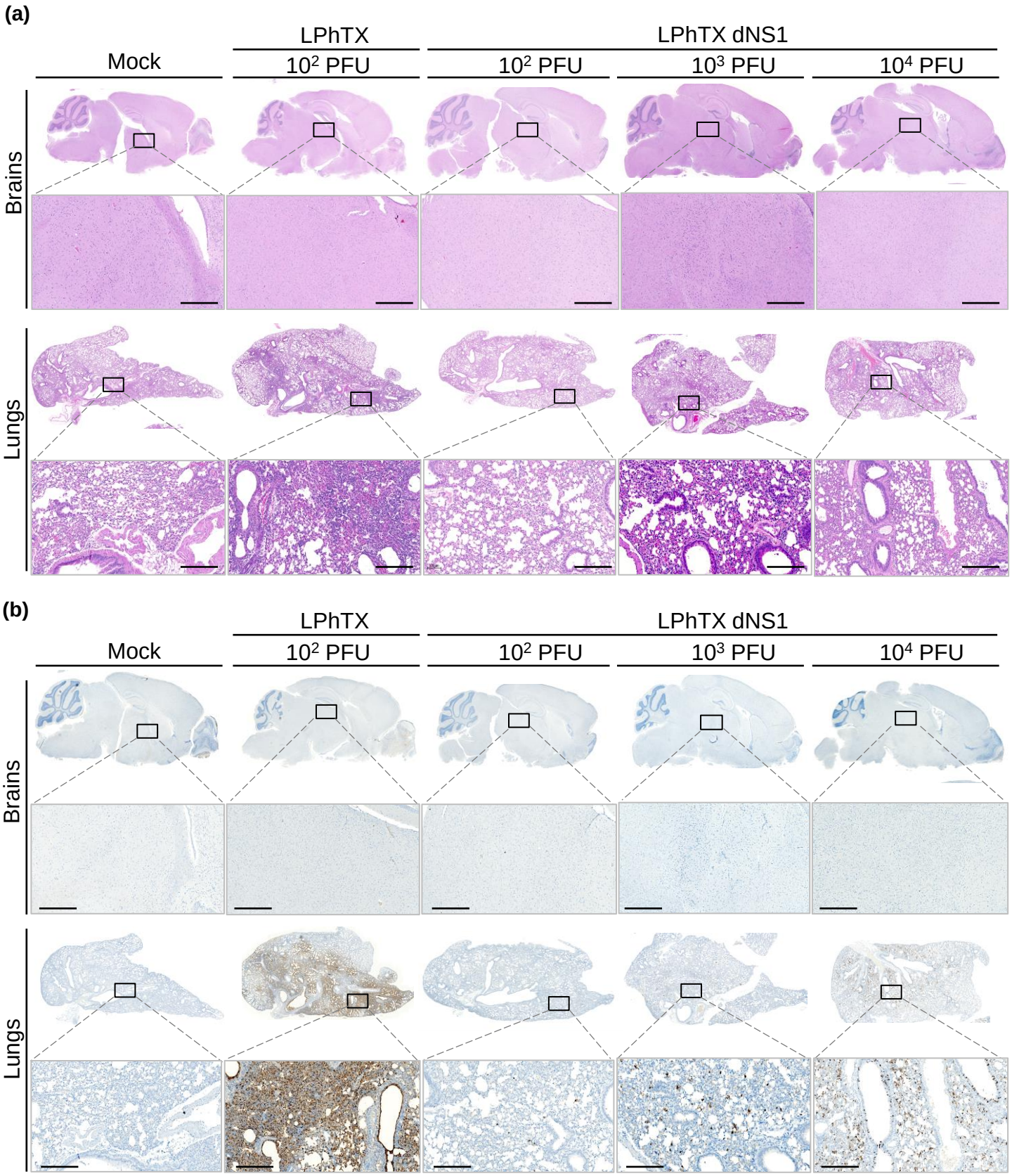
(a)
LPhTX
LPhTX dNS1
Mock
10^2 PFU
10^2 PFU
10^3 PFU
10^4 PFU
Brains
Lungs
(b)
LPhTX
LPhTX dNS1
Mock
10^2 PFU
10^2 PFU
10^3 PFU
10^4 PFU
Brains
Lungs

Figure 6

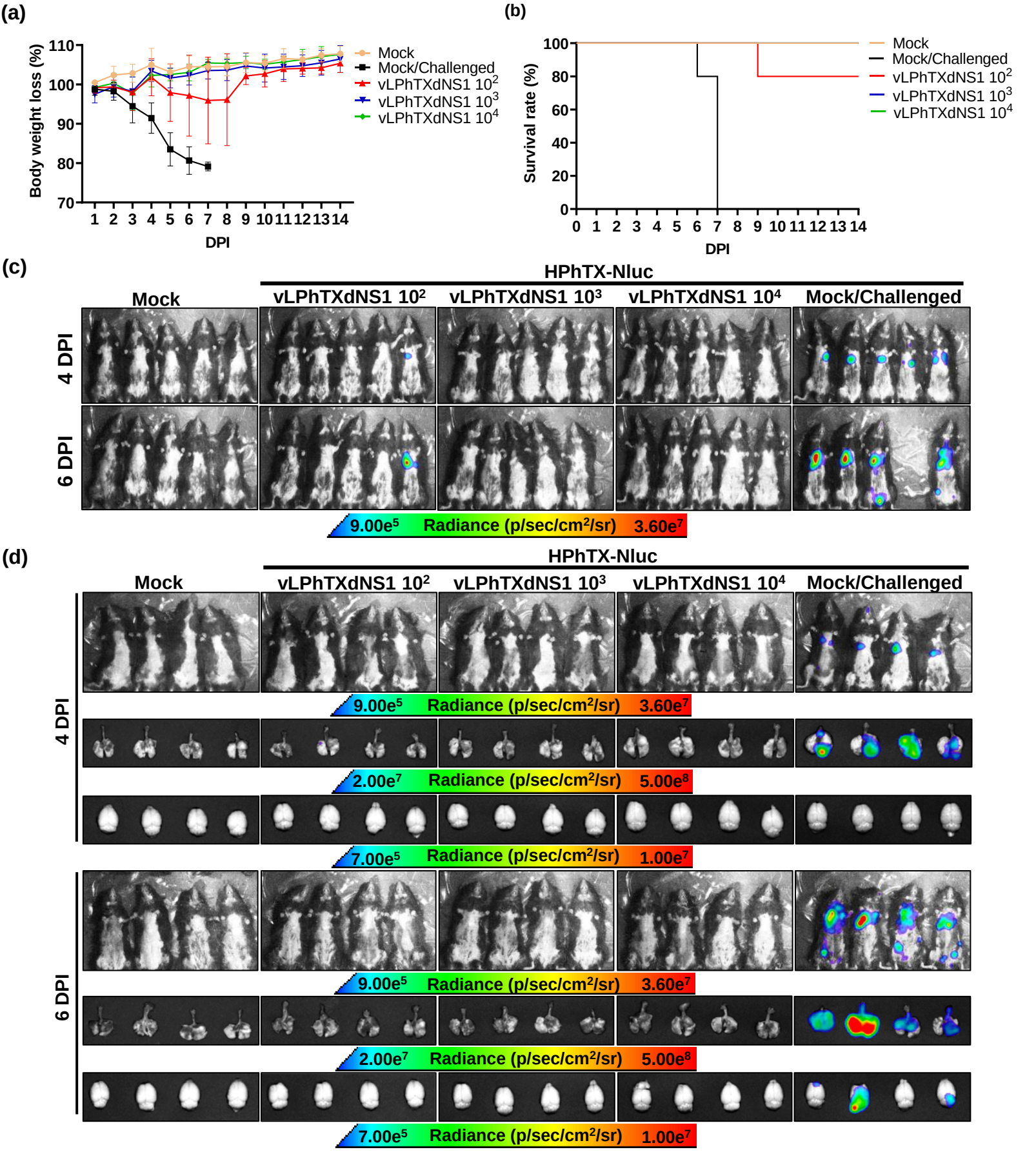
(a)
Body weight loss (%)
110
100
90
80
70
1 2 3 4 5 6 7 8 9 10 11 12 13 14
DPI
Mock
Mock/Challenged
vLPhTXdNS1 10^2
vLPhTXdNS1 10^3
vLPhTXdNS1 10^4
(b)
Survival rate (%)
100
80
60
40
20
0
0 1 2 3 4 5 6 7 8 9 10 11 12 13 14
DPI
Mock
Mock/Challenged
vLPhTXdNS1 10^2
vLPhTXdNS1 10^3
vLPhTXdNS1 10^4
(c)
HPhTX-Nluc
Mock
vLPhTXdNS1 10^2
vLPhTXdNS1 10^3
vLPhTXdNS1 10^4
Mock/Challenged
4 DPI
6 DPI
9.00e^5 Radiance (p/sec/cm^2/sr) 3.60e^7
(d)
HPhTX-Nluc
Mock
vLPhTXdNS1 10^2
vLPhTXdNS1 10^3
vLPhTXdNS1 10^4
Mock/Challenged
4 DPI
9.00e^5 Radiance (p/sec/cm^2/sr) 3.60e^7
2.00e^7 Radiance (p/sec/cm^2/sr) 5.00e^8
7.00e^5 Radiance (p/sec/cm^2/sr) 1.00e^7
6 DPI
9.00e^5 Radiance (p/sec/cm^2/sr) 3.60e^7
2.00e^7 Radiance (p/sec/cm^2/sr) 5.00e^8
7.00e^5 Radiance (p/sec/cm^2/sr) 1.00e^7

Figure 7

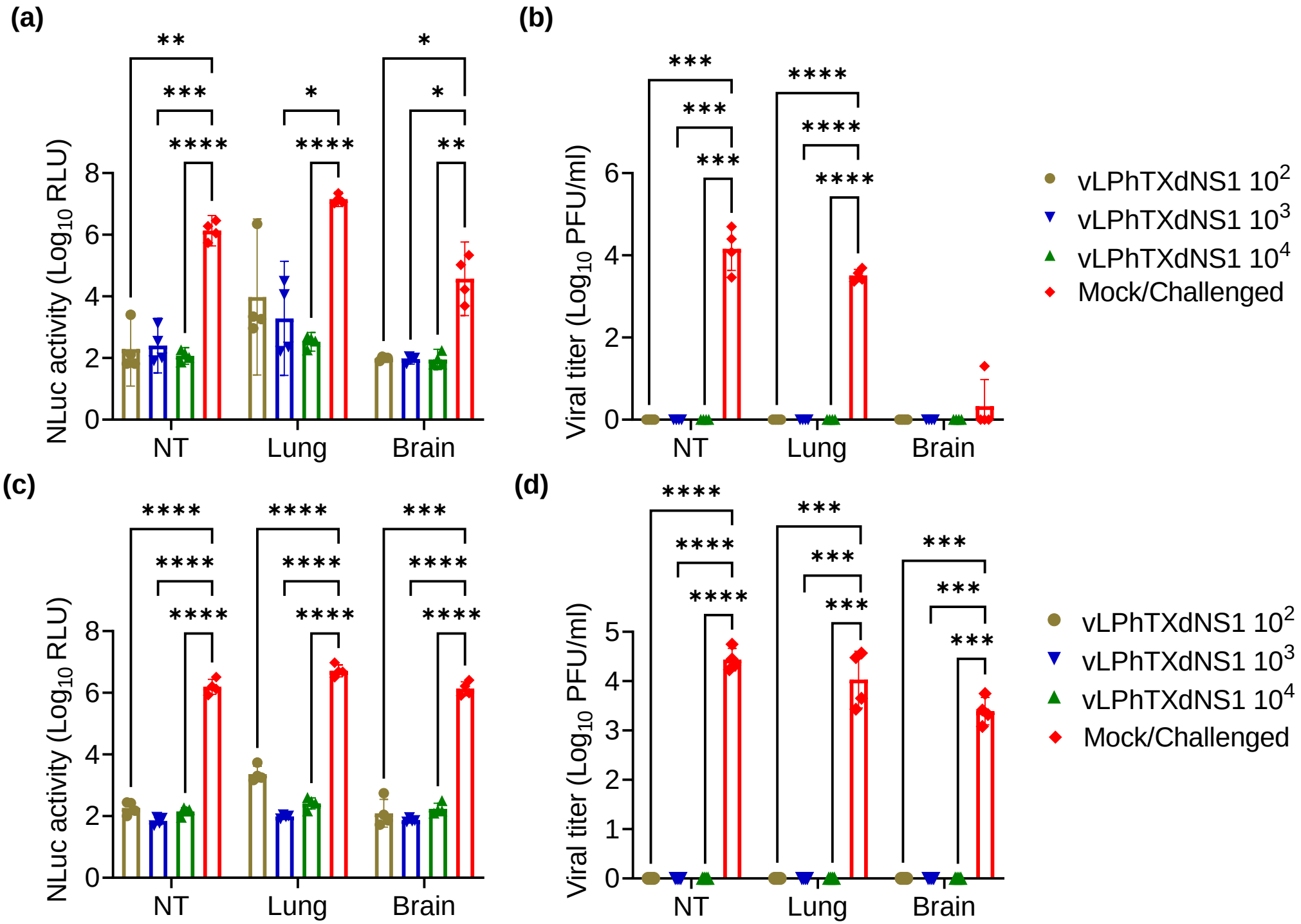
(a)
NLuc activity (Log10 RLU)
0
2
4
6
8
NT
Lung
Brain
**
***
****
*
****
*
*
**
(b)
Viral titer (Log10 PFU/ml)
0
2
4
6
NT
Lung
Brain
***
***
***
****
****
****
vLPhTXdNS1 10^2
vLPhTXdNS1 10^3
vLPhTXdNS1 10^4
Mock/Challenged
(c)
NLuc activity (Log10 RLU)
0
2
4
6
8
NT
Lung
Brain
****
****
****
****
****
****
***
****
****
(d)
Viral titer (Log10 PFU/ml)
0
1
2
3
4
5
NT
Lung
Brain
****
****
****
***
***
***
***
***
***
vLPhTXdNS1 10^2
vLPhTXdNS1 10^3
vLPhTXdNS1 10^4
Mock/Challenged

Figure 8

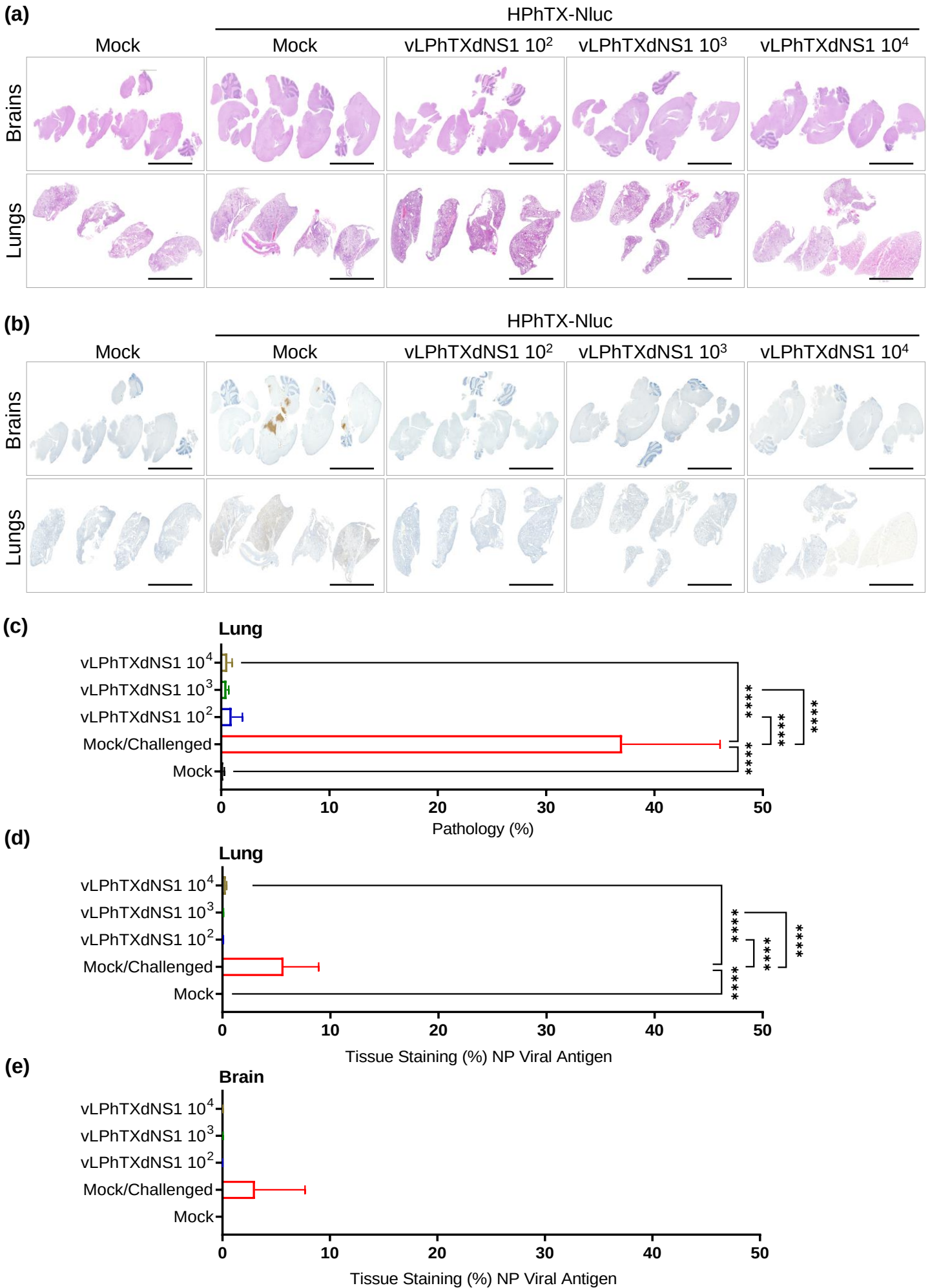
(a)
HPhTX-Nluc
Mock
Mock
vLPhTXdNS1 10²
vLPhTXdNS1 10³
vLPhTXdNS1 10⁴
Brains
Lungs
(b)
HPhTX-Nluc
Mock
Mock
vLPhTXdNS1 10²
vLPhTXdNS1 10³
vLPhTXdNS1 10⁴
Brains
Lungs
(c)
Lung
vLPhTXdNS1 10⁴
vLPhTXdNS1 10³
vLPhTXdNS1 10²
Mock/Challenged
Mock
0
10
20
30
40
50
Pathology (%)
(d)
Lung
vLPhTXdNS1 10⁴
vLPhTXdNS1 10³
vLPhTXdNS1 10²
Mock/Challenged
Mock
0
10
20
30
40
50
Tissue Staining (%) NP Viral Antigen
(e)
Brain
vLPhTXdNS1 10⁴
vLPhTXdNS1 10³
vLPhTXdNS1 10²
Mock/Challenged
Mock
0
10
20
30
40
50
Tissue Staining (%) NP Viral Antigen

Figure 9

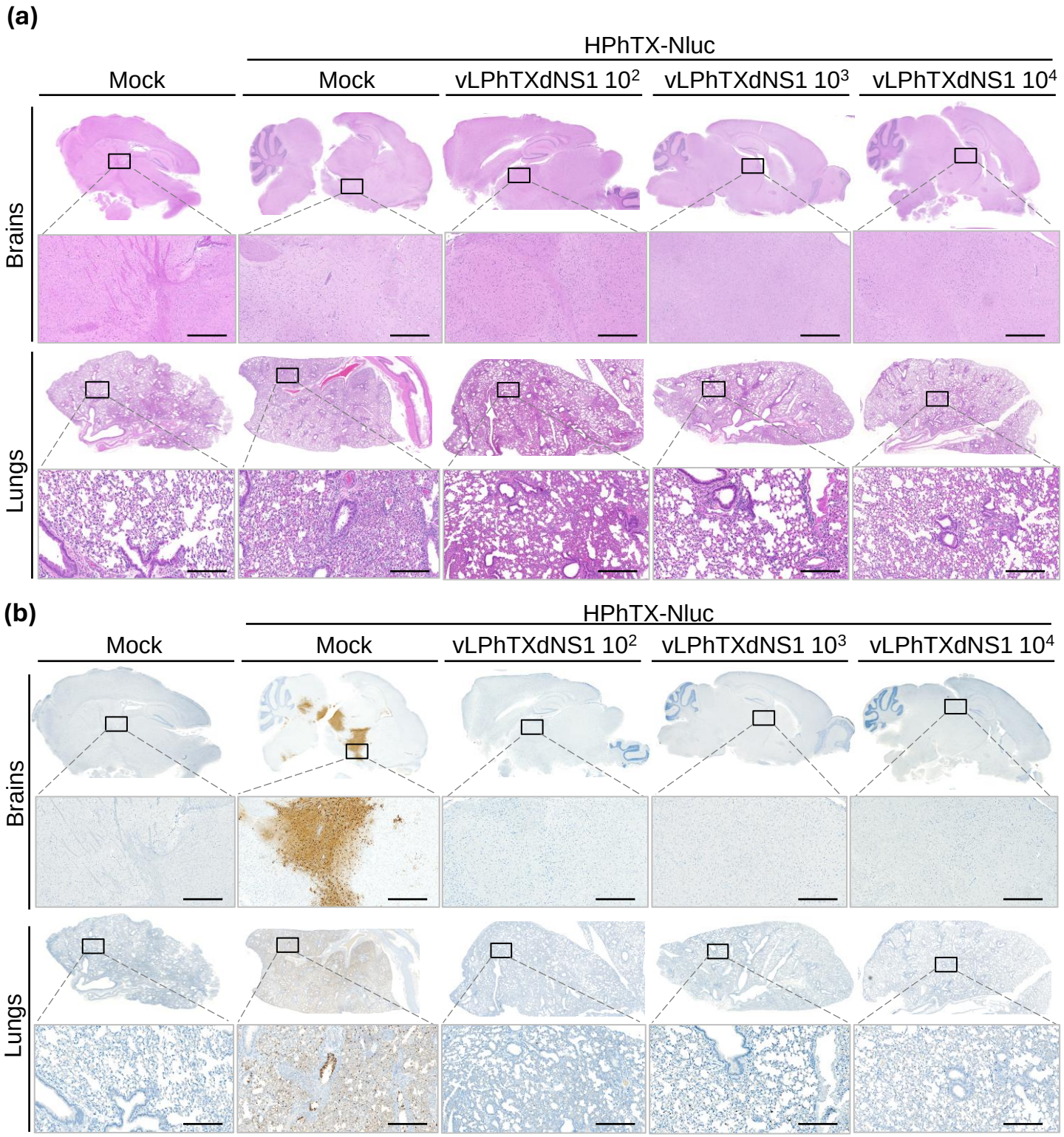
(a)
HPhTX-Nluc
Mock
Mock
vLPhTXdNS1 10²
vLPhTXdNS1 10³
vLPhTXdNS1 10⁴
Brains
Lungs
(b)
HPhTX-Nluc
Mock
Mock
vLPhTXdNS1 10²
vLPhTXdNS1 10³
vLPhTXdNS1 10⁴
Brains
Lungs